ISSN 2738-0971
eISSN 2738-1013

Bulletin of Natural Sciences Research

Vol. 13, N° 1-2, 2023.

BULLETIN OF NATURAL SCIENCES RESEARCH

Published by
Faculty of Sciences and Mathematics, University of Priština in Kosovska Mitrovica
Republic of Serbia

Focus and Scope

Bulletin of Natural Sciences Research is an international, peer-reviewed, open access journal, published semiannually, both online and in print, by the Faculty of Sciences and Mathematics, University of Priština in Kosovska Mitrovica, Republic of Serbia. The Journal publishes articles on all aspects of research in biology, chemistry, geography, geoscience, astronomy, mathematics, computer science, mechanics and physics.

Editorial Office

Ive Lole Ribara 29; 38220, Kosovska Mitrovica, Serbia, e-mail: editor@bulletinnsr.com, office@bulletinnsr.com; fax: +381 28 425 397

Printed by

Sigraf, Ćrila i Metodija bb, 37000 Kruševac, tel: +38137427704, e-mail: stamparijasigraf@gmail.com

Available Online

This journal is available online. Please visit http://www.bulletinnsr.com to search and download published articles.

BULLETIN OF NATURAL SCIENCES RESEARCH

Vol. 13, N^{o} 1-2, 2023.

CONTENTS

BIOLOGY

CHEMISTRY

MATHEMATICS, COMPUTER SCIENCE AND MECHANICS

Bulletin of Natural Sciences Research
Vol. 13, No. 1-2, 2023, pp. 1-4.

DOI: https://doi.org/10.5937/bnsr13-42787
Original Scientific Paper

RECORDS OF LICHEN SPECIES FROM GENUS ACAROSPORA, NEW FOR SERBIA, SOUTHWEST BALKAN PENINSULA

GORDANA ALEKSIĆ[1*], PREDRAG VASIĆ[1], TATJANA JAKŠIĆ[1]

[1]Faculty of Sciences and Mathematics, University of Priština in Kosovska Mitrovica, Kosovska Mitrovica, Serbia

ABSTRACT

The lichens: *Acarospora impressula, A. nitrophila, A. nodulosa, A. schleicheri, A. sinopica, A. smaragdula and A. umbillicata*, collected in North Kosovo are reported as a new species to Serbia, following a recent lichenological survey. Location, herbarium deposits and substrates are given, together with notes on distribution of the reported taxa.

Keywords: Lichens, New records, Biodiversity, Genus Acarospora, R. Serbia.

INTRODUCTION

Lichens biota are not well investigated in Republic of Serbia. A compilation of the greatest part of lichenological investigations in former Yugoslavia that includes the investigated area, was presented by Kušan. Kušan's work includes data from 1926 from Androssovsky and Szatala, who recorded 67 lichen species in the region of Kosovska Mitrovica (Kušan, 1953). Studies of lichens were carried out in the area of Kosovska Mitrovica during 1983, concluded "lichen desert" (Bejtullahuet al., 1983), while in 1988 the effects of polluted air on the lichens development in the same area (Murati et al., 1988) were investigated. The most complete contribution to lichens biota for the territory of the former Yugoslavia gave Murati (1992). Savić gave the data of lichen diversity in former Yugoslavia, researched the lichens in the mountain of Kopaonik (1996), investigated changes of the composition of epiphytic lichens in Belgrade area (1998a) and noted the presence of 43 taxa of lichens in Belgrade (1998b). The lichens were used as air pollution bio indicators in Belgrade area (Cvijan et al., 1997). The "lichen desert" boundaries changes in Belgrade has been monitored, compering the results of the research from 1980/81, 1991 and 2007 (Cvijan et al., 2008).The lichens of N.P. "Kopaonik" (Dimović & Jockić, 2000) and lichens of Radan Mountain (Dimović, 2001) has been investigated. "Checklist of the lichens of Serbia" contains 586 species. This checklist also contains a list of synonyms and faults records (Tibell & Tibell, 2006). Epithytic lichens have been used as indicators of the air quality in the urban part of Pirot city (Djekić et al., 2017). In the town of Zvečan epiphytic lichens have been investigated and their bio indicators value (Aleksic et al., 2019). Recently, the articles were published on records of lichenicolous fungi new for Turkey and Asia (Yazaciet al., 2019) and on lichens species new to Ukraine (Khodosovtsev & Darmostuk, 2020).

According to our literature survey, all six taxa presented in this work we register for the first time within the territory of Serbia, including Kosovo (Tibell & Tibell, 2006; Mayrhoferet et al., 2016). According to available data, it was the first lichen investigation at these sites (Tibell & Tibell, 2006).

MATERIALS AND METHODS

Study area

Lichen investigation was performed from October 2016 to January 2023, in the North part of Kosovo, i. e. Serbia,. In Zvečan 42°54'15.5"N, 20°50'47.36"E, alt. 700 m, Banjska (municipality Zvečan) 42°58'22.3"N, 20°46'57.0"E, alt. 547 m, Jagnjenica (municipality Zubin Potok) 42°55'14.4"N 20°45'29.0"E, alt. 680 m and Jarinje (municipality Leposavić) 43°13'17.3"N 20°42'02.7"E, alt. 480 m (Fig. 1).

North Kosovo zone has suitable habitats for lichens existence. The study area has various outcrops (granite, sandstone and limestone) as well as different type of woody plant species. The territory has agricultural landscape spatially.

Generally, about 83 % of the territory of Kosovo is characterized by humid climate and the rest of the territory is characterized by the semi-humid climate which is specific for the central part of the region and very-humid in the southwestern part of region. The spring is dominated by semi-humid climate 23.0. During the winter, values of indexes vary from 11.0. to a maximum of 28.0. As can be seen, most of Kosovo has humid conditions, except for small isolated area in the central part of Kosovo where is climate semi-humid. The summer season is mostly dominated by semi-arid climate conditions with values ranging from 10.0. to 20.0. Only parts of the south-western area are extremely humid. This season is the driest, based on average values of the indices, compared to the winter, spring and autumn values. Finally, the autumn is characterized by the humid but not very humid conditions >30.0. (Bačevićet al. 2017).

* Corresponding author: gordanaalekszic@gmail.com

Figure 1. Positions of the locations were the lichen species are investigated by KLM format, Google maps.

Standard microscopic techniques were used to identify the taxa of the collected samples up to species level. Morphological features were evaluated under a digital microscope, resolution 640x480 to 1600x1200. Same digital microscope was used to make photos for registered species. The identification of the lichen species was completed using the appropriate keys (Dobson, 2011; Wirth, 1995).

The collected lichen samples were deposited and recorded with matching vouchers, Herbarium of the Institute of Botany and Botanical Garden "Jevremovac", University of Belgrade (BEOU), (international abbreviation for the University of Belgrade Herbarium), Belgrade and in the private collection.

RESULTS AND DISCUSSION

1. *Acarospora impressula* Th. Fr. (Fig. 2).

Specimen examined: Jarinje, on exposed, Southern side of siliceous rocks, in the immediate vicinity of the administrative crossing, 18. March 2018. Aleksić G. (BEOU 409), private collection.

Distribution: In Britain and Ireland recorded at well-lit siliceous rocks, especially granite and also metal-rich sites, scares, mainly near the coast in the West (Dobson, 2011: 57); also reported from Italy (Nimis, 2016:30); Alps(Nimis, 2018: 15); Bulgaria (Denchev, 2022: 6).

Figure 2. *Acarospora impressula*.

2. *Acarospora nitrophila* H. Magn. (Fig. 3).

Specimen examined: Banjska, on the exposed, flat siliceous rock, in the vicinity of the medieval Banjska monastery, 2. October 2017; 5. February 2023, Aleksić G. (BEOU 638), private collection.

Distribution: Recorded former Yugoslavia as "very rare" for Macedonia, on siliceous (eruptive) rocks (Murati,1992: 73); in Britain and Ireland present on siliceous rock, especially if metal-rich, frequently occurs on the string courses and chamfers of churches (Dobson, 2011: 58); reported from Italy (Nimis,2016: 32); in Alps (Nimis, 2018: 15); in Bulgaria (Denchev, 2022: 6).

Figure 3. *Acarospora nitrophila*.

3. *Acarospora nodulosa* (Dufour) (Fig. 4).

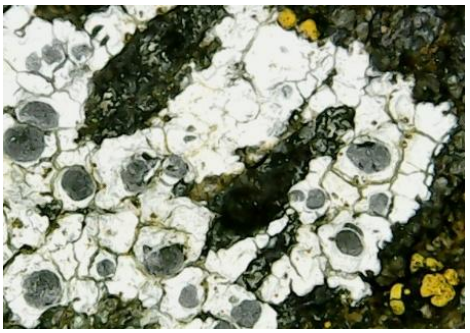

Figure 4. *Acarospora nodulosa*.

Specimen examined: Zvečan, on eruptive rocks, Northwest side, 3. March 2019; Jagnjenica, on the top of the rocky hill, 3. March 2019; Jarinje, on exposed, Southern side of siliceous rocks 15. April 2019, Aleksić G. (BEOU 260, 302, 303, 304/a, 365), private collection.

Distribution: Reported from Italy (Nimis, 2016:32); in Alps found in very open habitats (Nimis, 2018: 17).

4. ***Acarospora schleicheri*** (Ach.) A. (Fig. 5).

Specimen examined: Zvečan, prominent elevation, former volcano, on very dry siliceous rock, Southern exposure, 5. May 2018, Aleksić G. (BEOU 621).

Distribution: Recorded in former Yugoslavia as "very rare" for Macedonia, (Murati, 1992: 75); also known in Italy (Nimis,2016:33);widespread in Eurasia and North America; in the Alps confined to Inner-Alpine dry valleys (Nimis, 2018: 18).

Figure 5. *Acarospora schleicheri*.

5. ***Acarospora sinopica*** (Wahlenb.) Korb, (Fig. 6).

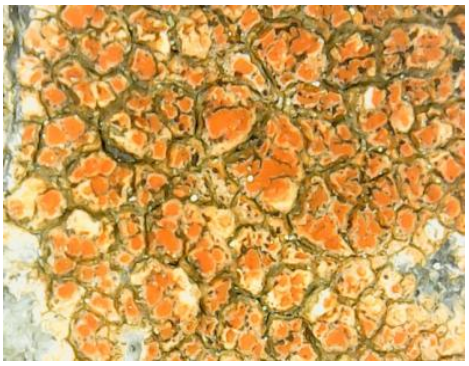

Figure 6. *Acarospora sinopica*.

Specimen examined: Jagnjenica, on the top of the rocky hill, 3. March 2019; 15. January 2023, Aleksić G. (BEOU 639), private collection.

Distribution: Known in Bulgaria (Murati, 1992: 74); fairly common in upland areas in Britain and Ireland, on iron-rich acid rock, often with *Tremolechia atrata*, *Rhizocarpon oederi* and *Lecanora epanora* (Dobson, 2011: 58); also, it has been reported from Italy (Nimis, 2016: 33); Alps as *Acarospora smaragdula* (Wahlenb.) A. Massal. var. *sinopica* (Wahlenb.) A. Massal. (Nimis, 2018: 19); Bulgaria (Denchev, 2022: 6).

6. Acarospora smaragdula (Wahlenb.) A. Massal. (Fig. 7).

Specimen examined: Zvečan, on top of a former volcano, widespread on very exposed eruptive rock, 2. April 2019, 12. January 2023, Aleksić G. (BEOU 366, 367, 368/a), private collection.

Distribution: Previously known in former Yugoslavia as "rare" for the Croatia, Macedonia, Bosnia (Murati, 1992: 74); present in Bosnia and Herzegovina (Bilovitz & Mayrhofer, 2010: 3); found in metal-rich situations like a walls, under metal grids, fairly common on siliceous rocks in Britain and Ireland (Dobson, 2011: 58).

Figure 7. *Acarospora smaragdula*.

7. ***Acarospora umbilicata***Bagl. (Fig. 8).

Specimen examined: Banjska, on the exposed flat siliceousrock,near the monastery Banjska, 26. October 2016; Zvečan, on exposed eruptive rock, 1. June 2018; Sendol, on the semi-shady part of the siliceous rock, 03. March 2019, Aleksić G. (BEOU 330, 369, 410).

Distribution: Reported for the Mediterranean region of the former Yugoslavia on exposed sites (Murati, 1992: 75);in Britain and Ireland mainly present on siliceous rocks and walls in seepage tracks from mortal and calcareous substrata (Dobson, 2011: 59); Italy (Nimis, 2016: 34).

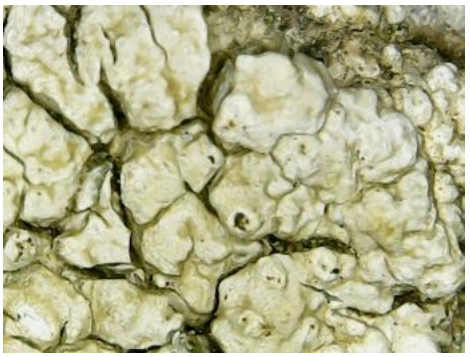

Figure 8. *Acarospora umbilicata*.

ACKNOWLEDGEMENTS

Author would like to thank to Dejan Živković, graduate engineer of electronics and telecommunications, for technical support.

REFERENCES

Aleksić, G., Stamenković, S., Ristić S. & Marković M. 2019. Epiphytic lichens in the town of Zvečan and their bioindicatior s value. The University Thought-Publication in Natural Sciences. 9(2), pp. 1-5. https://doi.org/10.5937/univtho9-19606

Bačević, N., Vukoičić, D., Nikolić, M., Janc, N., Milentijević, N. & Gavrilov, M. B. 2017. Adirity in Kosovo and Metohija, Serbia. Carpathian Journal of Earth and Environmental Sciences. 12(2), pp.563-570.

Bejtullahu, B., Beqiri, Sh. & Miletic, S. 1983. Ispitivanje zagađenosti vazduha Titove Mitrovice i okoline tokom 1982/83. god. Simpozijum o stanju, zaštiti i unapređenju čovekove sredine. Zvečan. pp. 153-164.

Bilovitz, P. O. & Mayrhofer, H. 2010. Catalogue of the Lichenized and Lichenicolous Fungi of Bosnia and Herzegovina. 51(1), pp. 1-67. Europe PMC Funders Group. Phyton.

Cvijan, M., Savić, S. & Szabados, K. 1997. Lichens as bioindicators of air pollution in Belgrade area. Ekologija. 32, pp. 99-106.

Cvijan, M., Subakov-Simić, G. & Krizmanić, J. 2008. Monitoring of the «lichen desert» in the Belgrade area (1980/81, 1991 and 2007). Archives of Biological Sciences. 60, pp. 215-222.

Denchev, C. M., Shivarov, V. V. Denchev, T. & Mayrhofer, H. 2022. Checklist of the lichenized and lichenicolous fungi in Bulgaria. MYCOBIOTA, 12(1), 106.

Dimović, D. & Jokić, M. 2000. Air quality control and the possibility of using lichen as a bioindicator of the state of the environment in the area of N.P. "Kopaonik". Proceedings of.the XXVIII Conference "Air Protection 2000". Serbian Air Purity Society. Belgrade. pp. 265-268.

Dimović, D. 2001. Lichens of Radan Mountain and surroundings - preliminary results. Protection of Nature. Belgrade. 52, pp. 107-113.

Djekic, T., Jaksic, T., Aleksic, G., Zivic, N., Markovic, M., Stamenkovic, S. & Ristic, S. 2017. Epithytic lichens as indicators of the air quality in the urban part of Pirot city (Southeastern Serbia) 2002-2014. Oxidation Communications, 40(4), pp. 1429-1442.

Dobson, F. 2011. Lichens An Illustrated Guide to the British and Irish Species. The Richmond Publishing Co. Ltd. England. pp. 496.

Khodosovtsev, A. Ye. & Darmostuk, V. V. 2020.Records of lichen species new for Ukraine from steppe habitats of the country. Botanica Serbica, 44(2), pp. 243-250.

Kušan, F. 1953. Prodromus flora of lichens of Yugoslavia. Yugoslav Academy of Sciences and Arts, Zagreb. 595 pp.

Mayrhofer, H., Czeh, D., Kobald, E-M. & Bilovitz, P-O. 2016. Catalogue of the lichenized and lichenicolous fungi of Kosovo. *Herzogia*. 29(2), pp. 529-554. DOI: 10.13158/heria.29.2.2016.529

Murati, M., Pejčinović, D. & Hodža, E. 1988. Uticaj o nečišćenog vazduha na razvoj lišajeva u području Titove Mitrovice. Četvrti kongres ekologa Jugoslavije. Ohrid.

Murati, M. 1992. Lichen flora of Slovenia, Croatia, Vojvodina, Bosnia and Herzegovina, Serbia, Montenegro, Kosovo and Metohija. University of Priština, Priština. 397 pp.

Nimis, P. L. 2016. The lichens of Italy, A second annotated catalogue. EUT, Trieste. pp. 740.

Nimis, P. L., Hafellner, J., Roux, C., Clerc, P., Mayrhofer, H., Martellos, S. & Bilovitz, P. O. 2018. The lichens of the Alps – an annotated checklist. MycoKeys, 31(1), 634.

Savić, S. 1995. Diversityof lichens of Yugoslavia with asurvey of species of international importance. In Stevanović, V., Vasić, V. (eds): Biodiverzitet Jugoslavije sa pregledom vrsta od međunarodnog značaja. Ecolibri & Biološki fakultet, Belgrade. pp. 151-157.

Savić, S. 1996. Lichen researches in the mountain of Kopaonik (1992-1993). Ekologija. Beograd. 31, pp. 55-62.

Savić, S. 1998a. Changes in the composition of epiphytic lichens in the Belgrade area (1981-1991). Ekologija. Beograd. 33, pp.65-70.

Savić, S. 1998b. Epiphytic lichens as bioindicators of air pollution in the area of Belgrade. Sauteria. 9, pp.331-340.

Tibell, S. & Tibell, L. 2006. Checklist of the lichens of Serbia. MycologiaBalcanica.Bulgarian Mycological Society, Sofia. 3, pp.187-215.

Wirth,V. 1995. Die Flechten Baden-Württembergs. 2 Bände. Stuttgart. pp.1006.

Yayaci, K., Etayo, J., Aslan, A. & Karahan, D. 2019. Records of lichenicolous fungi new for Turkey and Asia. BotanicaSerbica. 43(1), pp. 3-8.

Bulletin of Natural Sciences Research
Vol. 13, No. 1-2, 2023, pp. 5-9.
DOI: https://doi.org/10.5937/bnsr13-44767
Original Scientific Paper

DETERMINATION OF POLYPHENOL AND FLAVONOID CONTENT AND ANTIOXIDANT ACTIVITY OF ETHANOLIC, CHLOROFORM AND ETHYL ACETATE EXTRACT OF THE PLANT SPECIES *Thymus serpyllum* L.

MARIJA AKSIĆ[1*], BILJANA DEKIĆ[1], SUZANA JANIĆEVIĆ[1]

[1]Faculty of Sciences and Mathematics, University of Priština in Kosovska Mitrovica, Kosovska Mitrovica, Serbia

ABSTRACT

This research aimed to examine the phytochemical composition, content of polyphenols and flavonoids, and antioxidant capacity of ethanolic, ethyl acetate, and chloroform extract of the plant species *Thymus serpyllum* L. The extracts were tested for the presence of alkaloids, tannins, saponins, phenolic compounds, flavonoids, steroids, terpenoids, cardiotonic glycosides, and coumarins. The total content of polyphenols was determined spectrophotometrically with the Folin-Ciocalteu reagent, according to Singleton's method, while the total content of flavonoids was determined using the method with aluminum chloride. The highest contents of polyphenols and flavonoids were determined in ethanolic extracts, where the measured values ranged from 111.00 ± 0.26 to 288.00 ± 0.23 mg GAE/g of dry extract for polyphenols, and 65.80 ± 0.19 to 198.22 ± 0.34 mg RE/g dry extract for flavonoids. The antioxidant activity was determined by the DPPH (2,2-diphenyl-1-picrylhydrazyl) assay. The tested extracts show a good effect on DPPH radical inhibition, with the IC50 values ranging from 35.15 ± 0.33 to 398.27 ± 0.24 µg/ml, and the greatest ability of ethanolic extract to neutralize the DPPH radical. Qualitative phytochemical analysis of the extracts showed a wide spectrum of phytochemicals, where ethanol, as the most polar solvent, extracts almost all tested phytochemicals.

Keywords: *Thymus serpyllum*, Extracts, Polyphenols, Flavonoids, Phytochemicals, Antioxidant activity.

INTRODUCTION

Healing with herbs is as old as humanity itself. The positive impact of medicinal plants on human health is explained by the presence of secondary metabolites, for example, polyphenols, which can exhibit various biological activities, such as antimicrobial, antioxidant, and anti-inflammatory. Many compounds extracted from plants are used in medicine or represent a model for the production of numerous synthetic drugs with improved pharmacological effects (Živanović, 2015).

Among the aromatic plants belonging to the Lamiaceae family, the genus *Thymus* is noteworthy for its numerous species and varieties of wild plants. Thyme species are perennial, aromatic herbs and shrubs native to Europe, North Africa, and Asia. They are commonly used as culinary herbs and flavorings. Due to their antimicrobial, spasmolytic, and antioxidant effects, they are useful for medical purposes (Stahl-Biskup & Sáez, 2002), and also shows anti-inflammatory, antinociceptive, and antitumor effects (Mahmoudi et al., 2008; Nikolić et al., 2014).

Thymus serpyllum L. (wild thyme) is a highly valued medicinal and aromatic plant whose dried aerial part is used in traditional medicine and as raw material in the pharmaceutical industry. It acts as an antispasmodic, broncholytic, expectorant, diuretic, and sedative, and has antibacterial and antimicrobial effects (Kovačević, 2003). Wild thyme contains many flavonoid and phenolic antioxidants such as zeaxanthin, lutein, naringenin, luteolin, and thymonin. Fresh thyme has a high level of antioxidants and is full of minerals and vitamins that are essential for optimal health. Its leaves are one of the richest sources of potassium, iron, calcium, manganese, magnesium, and selenium (Sharangi & Guha, 2013). Based on the above, the goal of this research was to determine the total content of polyphenols and flavonoids, evaluate the antioxidant activity and determine the presence of certain groups of phytochemicals in the ethanolic, ethyl acetate, and chloroform extracts of the plant species *Thymus serpyllum* L. collected in the area of the Šar Mountains, Serbia.

EXPERIMENTAL

Materials and methods

Chemicals and reagents

Chemicals used in the experimental work was obtained from commercial sources and was used as purchased.

UV-Vis spectroscopy

All absorbance was measured using a LLG UniSPEC 2 spectrophotometer.

* Corresponding author: marija.aksic@pr.ac.rs

Plant material

Above-ground parts of the plant species *Thymus serpyllum* L. were collected in 2020 in the area of the Šar Mountains, Serbia. After 15 days of drying in the shade and in a drafty place, the plant material was packed in dark paper bags and stored in a dry and cool place until the analysis.

Preparation of extracts

Dried and well-ground plant material (5 g) was extracted with 100 ml of solvents of different polarity: ethanol, ethyl acetate, and chloroform, in a Soxhlet apparatus. The extraction carried out for 4 hours at the solvent boiling temperature. After the end of the extraction, the extracts were evaporated to dryness on a rotary vacuum evaporator, at a temperature of 40 ºC. The dry remains were transferred to vials and stored in a refrigerator at a temperature of 6 ºC until use. For analysis, the dry remains of the extracts were dissolved in methanol.

Determination of total polyphenol content

The total content of polyphenols in the tested extracts was determined spectrophotometrically with the Folin-Ciocalteu reagent according to Singleton's method, with minor modifications (Singleton et al., 1999). The work procedure was as follows: 0.5 ml (1000 µg/ml) of the methanol extract solution was measured in a test tube and 2 ml of Folin-Ciocalteu reagent (diluted ten times with distilled water) was added and mixed. After 3 minutes, 2.5 ml of 10% Na_2CO_3 solution was added and incubation was carried out at 25°C for 30 minutes. The absorbance was measured at 765 nm by comparing it with the blank sample (2 ml of Folin-Ciocalteu reagent was added to 0.5 ml of methanol, followed by 2.5 ml of 10% Na_2CO_3). The same procedure was repeated for the standard gallic acid solution, and the calibration curve was constructed based on different concentrations of gallic acid (7.81-500 µg/ml). Total polyphenol content was calculated from the calibration curve equation and presented in gallic acid equivalents as mg GAE/g dry extract.

Determination of total flavonoid content

The total content of flavonoids was determined spectrophotometrically, using the known method with aluminum chloride (Chang et al., 2002), with minor modifications. The working procedure was as follows: 0.5 ml (1000 µg/ml) of the methanol extract solution was measured in the test tube and 1 ml of methanol, 150 µl of 10% $AlCl_3$ solution, 150 µl of 1 M CH_3COOK solution, and 2.5 ml of distilled water were added. The contents were shaken and incubated at room temperature for 40 minutes. The absorbance was measured at 420 nm, by comparing it with the blank sample (having the same content, with replacing the standard solution of rutin and the tested extract with 0.5 ml of methanol). The same procedure was repeated for the standard rutin solutions (3.91-250 µg/ml) to construct the calibration curve. The flavonoid content was calculated from the calibration curve equation and expressed as rutin equivalent (mg RE/g of dry extract).

DPPH assay

To examine the antioxidant potential of the extracts of this plant species, we used the DPPH (2,2-diphenyl-1-picrylhydrazyl) method, using a modified procedure according to Farasat (Farasat et al., 2014). DPPH is a stable free radical with a delocalized free electron on the nitrogen atom, so the molecule does not form the dimers with most other free radicals. This delocalization allows for the appearance of a violet color, with an absorption maximum at 517 nm. When it receives one hydrogen from an antioxidant, it is reduced and turns into yellow DPPH-H, whereby absorption intensity at 517 nm decreases. This decrease is directly proportional to the antioxidant activity of the given substance (Figure 1).

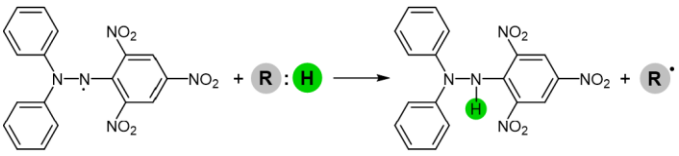

Figure 1. Mechanism of the reaction of DPPH radicals with antioxidants.

The working procedure was as follows: aliquots of 200 µl of the methanol solution of the extract of different concentrations (15.62, 32.25, 62.5, 125, 250, 500, and 1000 µg/ml) were placed in test tubes and mixed with 3 ml of a 0.004% methanol solution of DPPH. The test tubes were gently shaken and incubated for 35 minutes in a dark place at room temperature. Absorbance was measured at 517 nm. The blank sample contained methanol instead of the extract. The same procedure was repeated for the standard solution of ascorbic acid (1.96-125 µg/ml), which in our case was used as a benchmark for comparing the DPPH radical neutralization efficiency with the tested extracts, i.e., as a positive control. Inhibition of DPPH radicals in the presence of the tested sample is calculated by the formula and expressed in percent inhibition (%):

$$\% \text{ inhibition} = ((A-A_1)/A)\cdot 100$$

where A is the absorbance of the control sample (3 ml DPPH radical and 200 µl methanol), and A1 is the absorbance of the methanol extract solution (3 ml DPPH and 200 µl methanol extract solution). The IC_{50} value (µg/mL) can be calculated based on the equation of the calibration curve, which is obtained as a graphic representation of the dependence of the DPPH radical inhibition percentage on the concentration of the extract. EC_{50} "effective concentration" i.e., the IC_{50} value represents the concentration of antioxidants needed to reduce

the concentration of DPPH radicals by 50% (the lowest IC_{50} value corresponds to the highest free radical "scavenging" activity).

Statistical analysis

All analyzes were performed in triplicate and the results were statistically processed and expressed as mean value (n = 3) ± standard deviation. Statistical analyzes were performed with the help of GraphPad Prism ver. 7.00 and MS Office Excel (2016) software package.

Qualitative phytochemical analysis

During the examination of the phytochemical composition, the obtained ethanolic, ethyl acetate, and chloroform dry extracts were used as such or dissolved in a suitable solvent before certain phytochemical analyses. The extracts were tested for the presence of alkaloids, tannins, saponins, phenolic compounds, flavonoids, steroids, terpenoids, cardiotonic glycosides, and coumarins according to previously described methods (Sofowora, 1993; Trease & Evans, 2002; Harborne, 1973; Parekh & Chands, 2008; Kumar et al., 2013). These methods are based on the visual change in the color of the solution when specific reagents are added.

RESULTS AND DISCUSSION

Yield (%), total content of polyphenols and flavonoids

The yield of the obtained ethanolic, ethyl acetate, and chloroform extract of thyme ranges from 7.78 - 16.13 %. (Table 1). The highest yield during the extraction of plant material was given by ethanol as the most polar solvent (16.13%), while the yield of the chloroform extract was the lowest (7.78%).

Table 1. The yield of obtained extracts (%) of the plant species *Thymus serpyllum* L.

Extract	Ethanol	Ethyl acetate	Chloroform
Percentage yield % (w/w)	16.13	12.55	7.78

The concentration of total phenol content in the tested extracts was determined spectrophotometrically with the Folin-Ciocalteu reagent, and the values were calculated based on the equation obtained from the calibration curve. In a slightly basic medium, Folin's reagent with polyphenols gives a blue complex, whose concentration can be monitored spectrophotometrically, by measuring the absorbance on the 765 nm. The content of polyphenols in the examined extracts ranged from 111.00 ± 0.26 to 288.00 ± 0.23 mg GAE/g of dry extract (Table 2). The ethanol extract showed the highest concentration of phenolic compounds with a value of 288.00 ± 0.23 mg GAE/g dry extract, while the lowest value was measured in the chloroform extract (111.00 ± 0.26 mg GAE/g dry extract). The content of phenolic compounds in the ethyl acetate extract was 155.50 ± 0.14 mg GAE/g of dry extract. Based on numerous studies, it was seen that the total content of phenol in many plant species depends on the type of extraction, that is, on the polarity of the used solvents. Higher solubility of phenol in more polar solvents actually increases the concentration of phenolic compounds (Mohsen & Ammar, 2008; Zhou & Yu, 2004). For that reason, the total content of polyphenols in the ethanolic extract is higher, while in the chloroform extract it is the smallest. The total content of polyphenolic compounds, in our case, decreases in the expected order: ethanol > ethyl acetate > chloroform extract.

Table 2. Total content of polyphenolics and flavonoids of the plant species *Thymus serpyllum* L.

Extract	Total phenolics (mg GAE/g dw)	Total flavonoids (mg RU/g dw)
Ethanol	288.00 ± 0.23	198.22 ± 0.34
Ethyl acetate	155.50 ± 0.14	90.35 ± 0.27
Chloroform	111.00 ± 0.26	65.80 ± 0.19

The determination of the total content of flavonoids is based on their property to form complexes with metals. In this method, flavonoids form a complex with Al^{3+}, resulting in the formation of a yellow chelate. The concentration of flavonoids in the examined extracts of the plant species *Thymus serpyllum* L. ranged from 65.80 ± 0.19 to 198.22 ± 0.34 mg RE/g of dry extract (Table 2). The highest concentration of flavonoids was found in the ethanol extract (198.22 ± 0.34 mg RE/g dry extract), while the ethyl acetate and chloroform extracts showed lower concentrations (90.35 ± 0.27 and 65.80 ± 0.19 mg RE/g dry extract, respectively). As well as polyphenols, the total content of flavonoids depends on the polarity of the solvent (Min & Chun-Zhao, 2005). Therefore, the ethanolic extract has a higher content of flavonoids. In this sense, the content of flavonoids in our work decreases in the order: ethanol > ethyl acetate > chloroform extract.

The obtained results show that the examined extracts contain a smaller amount of flavonoids compared to phenolic compounds.

DPPH assay

The results showed that the tested extracts show a good effect on DPPH radical inhibition, with the IC_{50} value is in the range from 35.15 ± 0.33 to 398.27 ± 0.24 μg/ml (Table 3). The greatest ability to neutralize the DPPH radical was shown by the ethanolic extract, at a concentration of IC_{50} = 35.15 ± 0.33 μg/ml. The inhibition of the DPPH radical of the ethyl acetate extract (IC_{50} = 345.93 ± 0.10 μg/ml) is significantly lower, but still stronger in comparison to the chloroform extract (IC_{50} = 398.27 ± 0.24 μg/ml).

The IC_{50} values obtained in this way are in agreement with the results obtained for the total content of polyphenols

and flavonoids because they are known to have a strong antioxidant effect. Compared to ascorbic acid, which we know is a strong antioxidant (IC_{50} = 10.32 ± 0.16 μg/ml), we conclude that the ethanolic extract showed a high antioxidant potential.

Table 3. IC_{50} values of the tested extracts of the plant species *Thymus serpyllum* L.

Extract	DPPH assay IC_{50} (μg/ml)*
Ethanol	35.15 ± 0.33
Ethyl acetate	345.93 ± 0.10
Chloroform	398.27 ± 0.24

*Ascorbic acid was used as a positive control (IC_{50} = 10.32 ± 0.16 μg/ml)

The percentage of DPPH radical inhibition depending on the concentration of the tested extracts of the plant species *Thymus serpyllum* L. is shown in Figure 2.

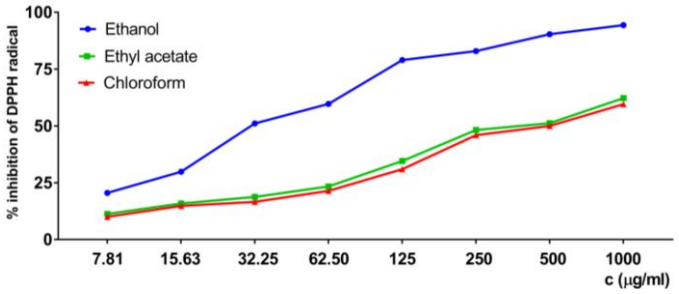

Figure 2. Percentage of DPPH radical inhibition depending on the concentration of the tested ethanolic, ethyl acetate and chloroform extract of thyme (*Thymus serpyllum* L.).

Qualitative phytochemical analysis

The examination of the qualitative phytochemical analysis showed a wide spectrum of phytochemicals in the tested extracts (Table 4). The ethanolic extract showed positive results for alkaloids, tannins, saponins, phenols, flavonoids, terpenoids, and coumarins, while the presence of steroids and cardiotonic glycosides was not confirmed. The ethyl acetate extract gave positive results for alkaloids, phenols, flavonoids, cardiotonic glycosides, and coumarins, and showed the absence of tannins, saponins, steroids, and terpenoids. The chloroform extract showed the presence of a smaller number of phytochemicals. This extract showed positive results for phenols, flavonoids, and cardiotonic glycosides, and no alkaloids, tannins, saponins, steroids, terpenoids, and coumarins were proven by the tests.

Based on the obtained results, we can conclude that the polarity of the solvent, as well as the nature of certain groups of phytochemicals, possess an important role during the extraction of plant material. Thus, ethanol, as the most polar solvent, showed the presence of almost all tested phytochemicals, while chloroform, as the least polar, showed the smallest number of phytochemicals.

Table 4. Qualitative phytochemical analysis of examined plant extracts.

Phytochemicals	Extract		
	Ethanol	Ethyl acetate	Chloroform
Alkaloids	+	+	–
Tannins	+	–	–
Saponins	+	–	–
Phenols	+	+	+
Flavonoids	+	+	+
Steroids	–	–	–
Terpenoids	+	–	–
Cardiotonic glycosides	–	+	+
Coumarins	+	+	–

CONCLUSION

Thymus serpyllum or wild thyme is a plant very useful for health and has been a synonym for folk medicine for many years. Medicinal ingredients in this plant are located only in the leaf and flower. This research showed that the extracts of this plant possess a high content of polyphenol and flavonoid compounds and significant antioxidant potential. Phytochemical analysis showed a large number of different groups of phytochemicals in all of the tested extracts. We can conclude that the presence of the phytochemicals in the extract depends on the polarity of the solvent used during the extraction. The results obtained in this work contribute to the knowledge about the antioxidant activity, and the content of polyphenolic and flavonoid compounds of the plant species *Thymus serpyllum* and, above all, will further influence the ethnopharmacological use of this plant species.

ACKNOWLEDGMENTS

This research was funded by the Ministry of Science, Technological Development and Innovations of Serbia [No. contract 451-03-47/2023-01/ 200123].

REFERENCES

Chang, C., Yang, M., Wen, H. & Chern J. 2002. Estimation of total flavonoid content in propolis by two complementary colorimetric methods, *J.* Food Drug Anal., 10, pp. 178-182. https://doi.org/10.38212/2224-6614.2748

Farasat, M., Khavari-Nejad, R. A., Nabavi, S. M. & Namjooyan, F. 2014. Antioxidant activity, total phenolics and flavonoid contents of some edible green seaweeds from Northern coasts of the Persian Gulf. Iran. J. Pharm. Research., 13(1), pp. 163-170. https://pubmed.ncbi.nlm.nih.gov/24734068

Harborne, J. B. 1973. Methods of plant analysis. In: Phytochemical Methods (Chapman and Hall) London.

Kovačević N. 2003. Basics of pharmacognosy. Belgrade: Institute for Textbooks and Teaching Aids.

Kumar, R. S., Venkateshwar, C., Samuel, G. & Rao, S. G. 2013. Phytochemical screening of some compounds from plant leaf extracts of *Holoptelea integrifolia* (Planch.) and *Celestruse marginata* (Grah.) used by Gondu tribes at Adilabad District, Andhra Pradesh, India, Int. j. eng. sci. invention res., 2(8), pp. 65-70.

Mahmoudi, M., Morteza-Semnani, K. & Mojra, E. 2008. Anti-inflammatory and antinociceptive activity of *Thymus pubescens* extract, Fitoterapia, 79(5), pp. 361-365. https://doi.org/10.1016/j.fitote.2008.04.004

Min, G. & Chun-Zhao, L. 2005. Comparison of techniques for the extraction of flavonoids from cultured cells of *Saussurea medusa Maxim.*, World J. Microb. Biot., 21, pp. 1461-1463.

Mohsen, M. S. & Ammar, S. M. A. 2008. Total phenolic contents and antioxidant activity of corn tassel extracts, Food Chem., 112, pp. 595-598.

Nikolić, M., Glamočlija, J., Ferreira, I. C. F. R., Calhelha, R.C., Fernandes, A., Marković, T., Marković, D., Giweli, A. & Soković, M. 2014. Chemical composition, antimicrobial, antioxidant and antitumor activity of *Thymus serpyllum* L., *Thymus algeriensis* Boiss. and Reut and *Thymus vulgaris* L. essential oils, Industrial Crops and Products, 52, pp. 183-190. https://doi.org/10.1016/j.indcrop.2013.10.006

Parekh, J. & Chands, S. 2008. Phytochemical screening of some plants from Western regions of India, Plant Arch, 8, pp. 657-662.

Sharangi A. B. & Guha S. 2013. Wonders of leafy spices: Medicinal properties ensuring Human Health. Sci.Int.. pp. 312-317.

Singleton, V. L., Orthofer, R. & Lamuela-Raventos, R. M. 1999. Analysis of total phenols and other oxidation substrates and antioxidants by means of Folin-Ciocalteu reagent, Methods Enzymol., 299, pp. 152-178. https://doi.org/10.1016/s0076-6879(99)99017-1

Sofowora, A. 1993. Medicinal Plants and Traditional Medicine in Africa, John Wiley and Sons Limited, 2: pp. 96-106.

Stahl-Biskup, E. & Sáez, F. 2002. *Thyme, the Genus Thymus*, Taylor and Francis, London, UK, 1st edition.

Stojčevski, K. 2011. Manual for growing medicinal and aromatic plants. Sokobanja: Association "Dr Jovan Tucakov".

Trease, G. E. & Evans, W. C. 2002. *Pharmacognosy*, 15th Edn. Saunders, pp. 214-393.

Zhou, K. & Yu, L. 2004. Effects of extraction solvent on wheat bran antioxidant activity estimation, LWT, 37, pp. 717-72. https://doi.org/10.1016/j.lwt.2004.02.008

Živanović-Turudija, S. 2015. Organization of production and processing of medicinal aromatic plants in Serbia, University of Belgrade, Faculty of Agriculture.

Bulletin of Natural Sciences Research
Vol. 13, No. 1-2, 2023, pp. 10-18.
DOI: https://doi.org/10.5937/bnsr13-44479
Original Scientific Paper

ASSESSMENT OF HEAVY METALS IN FISH AND SEDIMENTS FROM RIVER MTAKUJA IN THE VICINITY OF A GOLD MINE IN TANZANIA

VICTOR A. PANGA[1*], MWINGEREZA J. KUMWENDA[1], ISMAEL N. MAKUNDI[1]

[1]Physics Department, University of Dar es Salaam, P.o. Box 35063, Dar es Salaam, Tanzania

ABSTRACT

Concentrations of heavy metals namely Cr, Fe, Cu, Zn, As, Cd and Pb in African Sharptooth Catfish (*clarias gariepinus*) and sediment from river Mtakuja Tanzania were analyzed using the Energy Dispersive X-ray Fluorescence spectrometry technique. 32 samples from fish and sediment were investigated. The results show that the concentration of heavy metals was higher in upstream areas than in the downstream area. The concentration of Fe of 428.5 mg/kg in catfish from the upstream area was about 2 times 243.8 mg/kg obtained from the same fish in the downstream area. Similar cases observed for sediments with Fe concentration of 127626.9 mg/kg from upstream that was about 6 times higher than that of 21460.3 mg/kg from downstream area. The concentration of 44.8 mg/kg for Cu in the upstream area sediment was also about 2 times higher than 23.2 mg/kg in the downstream area sediment, while for as the concentration of 13.2 mg/kg was measured in the upstream, which is which is more than 5 times 2.5 mg/kg measured in downstream. The concentration of Cr in the catfish was 17.6 mg/kg which is higher than the permissible limit values of 0.8 mg/kg set by the European Commission (EC), 0.2 mg/kg set by the Food and Agricultural Organization (FAO) and 0.15 mg/kg the World Health Organization (WHO) limit. Moreover, the concentration of Cd was 3.0 mg/kg, which is above the permissible level of 0.2 mg/kg recommended by the EC and WHO. A positive correlation exists between the Cu, Pb, Fe and Cd concentration found in sediments and fish samples. The results show that the river Mtakuja is polluted by mining waste, domestic and agrochemical activities. This suggest that, there is a need for regular monitoring of heavy metal in river Mtakuja in order to monitor and protect aquatic organisms and health of benefactors of this river.

Keywords: Heavy metals, Energy Dispersive X-ray Fluorescence, African Sharptooth Catfish, Gold mine.

INTRODUCTION

Heavy metals refer to elements having specific gravity/density greater than 4 or 5 g/cm3 (Jaishankar et al., 2014). Moreover, heavy metals include Cadmium (Cd), Lead (Pb), Copper (Cu), Zinc (Zn), Arsenic (As) and Chromium (Cr) which are mainly dependent on chemical properties rather than specific gravity (Duruibe et al., 2007). Some heavy metals are essential to living organisms while others such as As, Cd and Pb are non-essential and toxic even at a low level of exposure (Wang et al., 2020). These metals can be released into the environment as byproducts of human activities including mining operations, domestic sewage, industrial waste, oil spills, combustion of biomass, and the use of fertilizers, pesticides and disease control agents in plants (Okereafor et al., 2020). The emission of heavy metals leads environmental pollution in air, lands and water such as rivers and lakes which are considered environmental hazards for invertebrates, fishes and humans.

The heavy metal contaminants in aquatic ecosystems being in soluble or suspension form tend to settle down at the bottom and be ingested by plants and animals or absorbed by sediments (Baby et al., 2010; Opaluwa et al., 2012). In the aquatic ecosystem, 99% of the heavy metal contaminants are stored in the sediments (Shen et al., 2019). Heavy metals in the sediments cause detrimental impacts that can change the aquatic ecosystem and can reach the food chain through plants and aquatic animals (Mataba et al., 2016). Among the inhabitants of the aquatic ecosystem that are largely affected by the detrimental impacts of the heavy metal pollutants are fish (Baby et al., 2010). Generally, fish can be used to assess the environmental health of the aquatic ecosystem and bio-accumulation of heavy metals is known to depend on the nature of the aquatic environment, type of heavy metal, rate of absorption, deposition and excretion (Miri et al., 2017; Mielcarek et al., 2022). As a result, sediments and fish are commonly used as good indicators of contamination levels in aquatic environments (Opaluwa et al., 2012; Mataba et al., 2016).

Different analytical techniques can be used for the analysis of heavy metals in materials. The commonly used techniques include Atomic Absorption spectrometry (AAS), Inductively Coupled-Plasma Mass Spectrometry (ICP-MS), Neutron Activation Analysis (NAA), Particle-Induced X-ray Emission (PIXE) and Energy Dispersive Spectroscopy (EDXRF). In comparison to other approaches, quantitative and qualitative analysis of sample with EDXRF are performed without any chemical manipulation, less time-consuming in

* Corresponding author: victorpanga996@gmail.com

terms of sample preparation and analysis, also uses low cost consumables (Eser et al., 2014). The EDXRF is also a non-destructive technique with high resolution potential for accurate determination of the broad elemental composition of samples from parts per million (ppm) to 100% by weight (Ravisankar et al., 2015; Perring et al., 2017). Furthermore, the EDXRF is a mature technique that is widely applied in many fields including geology, metallurgy, environment, ecology, mining, art sciences, fuel industries, jewelry, medicine, forensic sciences, agriculture, food industry and cosmetics (Perring et al., 2017; Nuchdang et al., 2019).

Mining processes at the Geita Gold Mine (GGM) have posed concerns about the heavy metal pollution to the environment and health (Nyankweli, 2012). The wastes, tailings and effluents from different stages of mineral processing are discharged into the environment resulting to contamination of soil, sediments, air, water and plants (Bitala, 2008; Almås & Manoko, 2012). River Mtakuja is located in downstream area of the GGM and it is the home to different fish species including Nile-Perch (*latesniloticas*), Lungfish (*protopterus aethiopicus*) and African Sharptooth Catfish (*clarias gariepinus*). The catfish is the common fish in river Mtakuja that is also largely consumed by the local community. The Catfish is also known to bio-accumulate heavy metals in a significant amount in the tissue and for a long time (Opaluwa et al., 2012). Furthermore, it has been proposed that the mining operations result to pollution of the aquatic ecosystem of river Mtakuja that is flowing toward Lake Victoria (Bitala, 2008). Moreover, Mtakuja river is a receptor of leaching contaminants from mining activities (Nyankweli, 2012). However, the reports on heavy metals contamination levels in both fish and sediments from the river Mtakuja are still marginal in literature. This means that consumption of fishes from Mtakuja river might pose environmental and health risks to the population. In an effort to overcome some of these challenges, this paper reports the results from the assessment study of the heavy metals in African Sharptooth Catfish (*clarias gariepinus*) and sediments from the river Mtakuja in the proximity of the gold mine. The results provided are significant towards establishments of control measures and monitoring the pollution levels of heavy metals from the river Mtakuja.

MATERIALS AND METHODS

Description of the study area

River Mtakuja is located between the latitude 02° 53′ 1.854″ to 02° 47′ 0.588″ S and longitude 32° 11′ 16.302″ to 32° 4′ 0.018″ E as shown in Fig.(1). It is a shallow river formed by different tributaries from the upper Geita forest. The aquatic ecosystem is bounded by thick forests and seasonal swamps in the upper zone which is only 0.5 km from Geita Town while the permanent swamp is located in the lower zone neighboring Lake Victoria. The river receives effluents from the GGM, municipal, domestic and agricultural runoffs, and pours water into Lake Victoria (Emel et al., 2014).

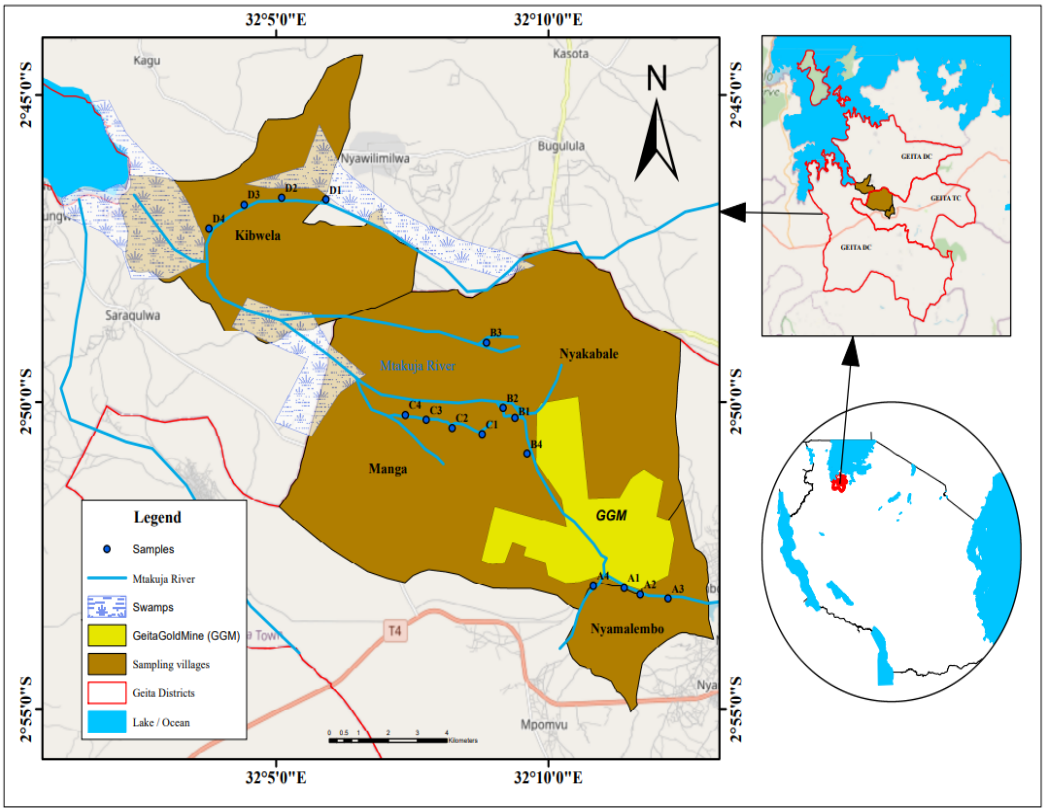

Figure 1. Map of Geita showing sampling areas.

Sampling and sample preparation

The river Mtakuja was divided into two zones, namely, upstream and downstream zones. The upstream zone consists of Nyamalembo, Nyakabale and Manga villages whereas the downstream zone consists of Kibwela village. In this study, 16 sediment and 16 fish samples were collected at different locations along the river Mtakuja as indicated in Fig.(1). At Nyamalembo samples of both sediments and fish were taken at locations marked A1, A2, A3 and A4, while at Nyakabale samples were taken at location marked B1, B2, B3 and B4, at Manga, samples were collected from location marked C1, C2, C3 and C4 and from Kibwela samples were collected at locations marked D1, D2, D3 and D4 (Fig. 1). Samples of catfish (*clarias gariepinus*) were taken directly from the river, then washed with distilled water to remove external dirt. Sediment samples (100 g) were collected from surface sediments at a depth ranging between 2 – 25 cm by scooping with a stainless steel spoon from the location where fish samples were taken. Since the sediments and fish samples were taken from the same locations, the distances from one sampling points to another were not equal.

The samples of fish and sediments were immediately placed in polythene bags, labeled and stored at a temperature ranging between -10 and 0 ^{0}C in a cooler box. Both samples were transferred to the University of Dar es Salaam in Dar es Salaam, Physics laboratory for further preparation. In the laboratory fish samples were dissected and bones removed to remain with tissue (gill, liver and muscle). The samples were then placed in a drying oven for 48 hours at a temperature between 45 – 50^{0}C (Mohamed et al., 2016). Thereafter, samples were crushed into small grains using a mortar and pestle for five (5) days and ground using the electric grinder for three (3) days to obtain a fine powder.

Figure 2. Image of pelletized samples ready for analysis.

The powder sample was sieved using an electric shaker to reduce particle size for five (5) days and placed in polythene bags with labeling, this procedure was repeated for all 32 samples. All samples were transferred to the Tanzania Atomic Energy Commission (TAEC) in Arusha for analysis. A wax binder was used in both samples to ensure homogeneity where 4 g powder was mixed thoroughly with 0.9 g of a binder. The sample was then pulverized until a homogenous mixture was obtained using a vortex mixture machine, then pressed using a hydraulic press at a pressure of 15 bar for one minute to obtain smooth pellets as shown in Fig. (2).

Sample analysis

The collected sample was analyzed for seven heavy metals namely Cr, Fe, Cu, Zn, As, Cd and Pb. The measurements were done using the EDXRF (XEPOS^{TM} bench-top spectrometer) equipped with the X-ray tube and three secondary targets, HOPG crystal, Al_20_3 and Mo. Pellets were placed in the EDXRF machine and irradiated for 15 minutes, the machine has six active holes where the sample was placed for each analysis. The X-ray tube was operated at a voltage range of 20 to 50 kV and a current varying between 0.1 and 1 mA depending on the target. The resulting spectra were processed using Turbo quant software. The X-lab Pro^{TM} software with turbo quant (Tq 9232) installed in the PC was used to correct the interference noises and background effects of a spectral line using the fundamental parameter-method. Accurate correction of the software was achieved by converting the intensities of the X-ray radiation into the concentration of an element C_i based on Eq. (1) (Mohamed et al., 2016).

$$C_i = K_i \times I_i \times M_\alpha \quad (1)$$

where, K_i is the proportionality constant, I_i is the intensity of fluorescent radiation in counts per second and M_α is the correction factor for the matrix effect.

Statistical analysis software

Statistical analysis of data was accomplished using the origin software (version: 2019b 9.65). P values less than 0.05 were considered statistically significant. Correlation between the investigated element in sediment and fish was performed by using the Pearson correlation coefficient. In addition, the MS excel spreadsheet 2013 was also used to store and process statistical data.

RESULTS AND DISCUSSIONS

Minimum detection limit

The minimum detection limit (MDL) is the smallest amount of the analyte that can be detected by the machine in a specified context for a given matrix with a 95 % confidence level (Kadachi & Al-Eshaikh, 2012). MDL is the quantity of the analyte that provides a net line intensity equal to three times the standard counting error of the background intensity (Rousseau, 2001). Detection limits are lower when the measuring time is higher and with increasing tube voltage and

anode current (Kadachi & Al-Eshaikh, 2012).The *MDL* was determined automatically by using X-Lab Pro Software based on Eq. (2) (Rousseau, 2001).

$$MDL = \frac{3 \times C_i}{I_p - I_b} \cdot \sqrt{\frac{I_b}{T_b}} \quad (2)$$

where, C_i is the concentration of the analyte *i* in % or ppm, I_p is the peak intensity, I_b is the background intensity and T_b is the background counting time. The minimum detection limits of the analyzed elements by using the EDXRF in this study as presented in (Table 1).

Table 1. MDL (mg/kg) of the analyzed elements from fish and sediment samples.

Chemical symbol	Atomic number	Fish	Sediment
Cr	24	5.6	18.8
Fe	26	2.4	5.0
Cu	29	0.9	2.0
Zn	30	1.0	0.9
As	33	0.3	1.4
Cd	48	4.1	5.6
Pb	82	0.7	1.6

Mean concentration of heavy metals in catfish (Clarias gariepinus)

The mean concentration of heavy metals in African Sharptooth Catfish (*Clarias gariepinus*) from upstream and downstream areas of river Mtakuja are presented in (Table 2).

Table 2. Measured mean concentration levels of heavy metals in catfish from the upstream and downstream areas of Mtakuja river.

Element	Concentration ± Standard Deviation (SD) (mg/kg)	
	Polluted areas (Upstream) (n = 60)	Clean area (Downstream) (n = 20)
Cr	17.6 ± 2.1	16.9 ± 1.8
Fe	428.5 ± 3.9	243.8 ± 3.4
Cu	2.7 ± 0.1	14.6 ± 0.5
Zn	38.3 ± 1.2	32.5 ± 0.9
As	0.2 ± 0.01	0.2 ± 0.01
Cd	3.0 ± 0.05	2.9 ± 0.05
Pb	0.3 ± 0.02	0.3 ± 0.02

The results show that the highest concentration is recorded for Fe and the lowest concentration is recorded for As. The mean concentration of the heavy metals in catfish from upstream area follows the order, Fe > Zn > Cr > Cd > Cu >Pb> As. Meanwhile, the downstream concentration levels are is in the following order, Fe > Zn > Cr > Cu > Cd >Pb> As.

The results show that the average concentration levels of Cr, Fe, Zn and Cd in catfish are slightly higher in the samples collected from upstream areas than those from the downstream areas (Table 2). This implies that the upstream areas of river Mtakuja are more polluted by the mining activities than the areas in the downstream of the river. The concentration of Fe in the upstream area is about 2 times more than that of the downstream area. However, the concentration of Cr, Zn and Cd from the upstream area show significant deviation to that of the downstream. Results of the non-essential elements As and Pb did not show any difference in upstream and downstream concentration levels, while Cu recorded a concentration of more than 5 times in the downstream area compared to the upstream area.

Iron is the 4th most abundant element in the earth's crust, it naturally occurs in rocks inform of sulphides such as pyrite (FeS_2) (Nkuli, 2008). Despite the natural phenomenology of iron that increase its concentration in water bodies and sediments, a higher concentration of iron recorded in this study can be linked to anthropogenic activities including mining and the presence of human settlements along the river Mtakuja that discharge domestic and industrial wastes into the river. The elevated mean concentration of Zn recorded is associated to the fact that most of the Zn compounds are largely soluble in water, therefore easily absorbed by aquatic organisms such as fish. Moreover, Zn occurring naturally in rocks such as sphalerite (ZnS) are easily exposed to the rock surfaces by anthropogenic activities such as mining activities. Moreover, weathering and abrasion of rocks, zinc galvanized objects, domestic and industrial discharge might also cause an increase in concentration levels of Zn in sediments and fish.

Copper and lead are released into the aquatic ecosystems due to runoffs from agricultural activities and the use of agrochemicals containing heavy metals. Cu and Pb are also found naturally in the sulphide rocks in form of chalcopyrite ($CuFeS_2$) and galena (PbS), respectively, which are released into the marine environments by weathering of rocks and mining operations. The concentration levels of Pb measured was below the detection limit of the EDXRF machine for fish samples (Table 1)and the presence of Cu can be attributed to the activities of GGM and agricultural activities along the river Mtakuja. A high concentration of Cu in the downstream area is associated to a large agricultural field at Kibwela village where runoffs during the rainy season increase the concentration of Cu in this river. Cadmium originates from large cadmium-based batteries commonly used in mining industries and

agricultural run-offs where phosphate fertilizers are used (Opaluwa et al., 2012). The presence of Cd in any aquatic ecosystem indicates intolerable contamination level. Cadmium concentration levels were however below the detection limit of the EDXRF for both fish and sediment samples.

Arsenic is naturally found in sulphide ores containing gold minerals commonly in the form of arsenopyrite (FeAsS) and realgar (As_4S_4) (Almås & Manoko, 2012). In this study, the concentration of arsenic was below the detection limit for fish samples. However, its presence in sediments originates from the leaching of the tailing waste due to the activities of the GGM. Dissolved arsenic is transported in the leachate ending in the aquatic environment where it is absorbed by the fish species. Chromium naturally occurs in rainwater, seawater, surface water and ground water, and in minerals where manmade activities such as mining become the major source of Cr in aquatic environments (Vaiopoulou & Gikas, 2020). Figure 3 presents the variation of the concentration levels of heavy metal in fish from the upstream and the downstream areas of Mtakuja river.

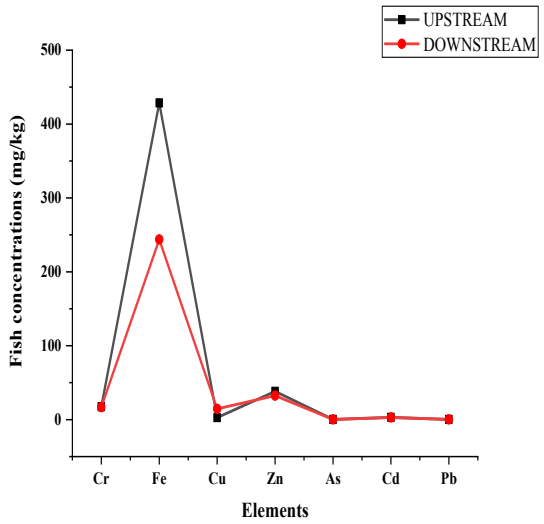

Figure 3. Variation of concentration of heavy metals in fish from upstream and downstream areas.

Mean concentration of heavy metals in sediments

The mean concentration levels of heavy metals in sediments collected from upstream and downstream areas of river Mtakuja are shown in (Table 3). The highest concentration level in the sediment samples from the upstream area was recorded for Fe and the least concentration recorded for Cd. Higher levels of Fe, Cu, Cr, Zn and As were obtained in sediment samples collected from upstream than those from downstream areas (Table 3). The concentration of Fe in the upstream area is about 6 times higher than the concentration of the elements in the downstream area. The concentration of Cu in the upstream area is about 2 times that of the downstream area, and that of As is more than 5 times higher in the upstream than in the downstream. The concentration of Cr and Zn are slightly higher in the upstream area than the concentration levels in the downstream area. Notably, the concentration levels for Cd and Pb are also significant in upstream and downstream areas. Variation of heavy metal concentration levels between the upstream and downstream areas can be associated to the proximity distance from the source of contamination. The separation between the contaminated area and contamination source is known to influence the concentration of heavy metals (Bitala, 2008). Furthermore, dissolved elemental concentration levels are expected to be low in the downstream area which is far from the mine due to the absorption of the sediment that reduces the elements from the water column (Mataba et al., 2016). The variation in the concentration of heavy metals in sediments in the upstream and downstream areas of the river Mtakuja is shown in Fig. (4).

Table 3. Concentration of heavy metals obtained in sediments from the upstream and downstream areas.

Element	Concentration ± Standard Deviation (SD) (mg/kg)	
	Polluted areas (Upstream) (n = 60)	Clean area (Downstream) (n=20)
Cr	39.4 ± 2.3	30.0 ± 2.1
Fe	127626.9 ± 221.4	21460.3 ± 51.2
Cu	44.8 ± 3.2	23.2 ± 1.8
Zn	32.0 ± 1.5	28.3 ± 0.9
As	13.2 ± 1.0	2.5 ± 0.2
Cd	4.4 ± 0.3	4.7 ± 0.3
Pb	21.8 ± 1.1	27.8 ± 1.0

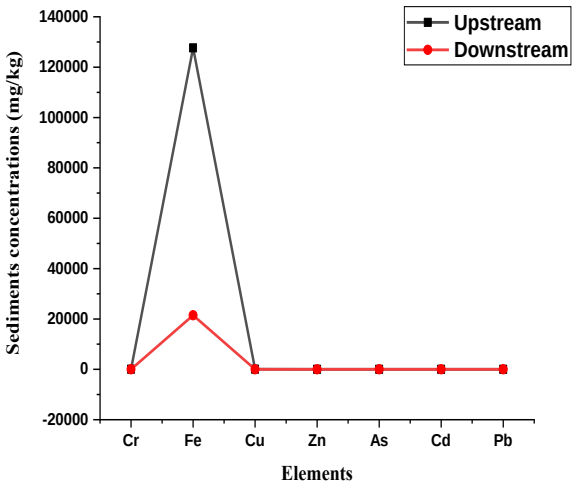

Figure 4. Variation of concentration of heavy metals in sediments from upstream and downstream areas.

The trends of the results show that the concentration levels of heavy metals in fish and sediments are higher in upstream areas than downstream areas of river Mtakuja (Figs. 3 and 4). For evaluation, the pictures of acid mine drainage and tailing rocks and other mining wastes along the river Mtakuja are shown in Figure 5. These pictures reveal compelling reason due to the indication of the Acid Mine Drainage (AMD) from the upstream area of the river Mtakuja especially in slow-moving waters as shown in Fig. 5. (a). The AMD is formed from sulphide oxidation products after it has been accumulated on rock surface by the mining process (Casiot et al., 2009). The acidic water dissolves heavy metals and transports them into water bodies. Sediments absorb heavy metals when pollutants are dissolved and discharged into water surfaces (Candeias et al., 2018). Moreover, the presence of tailing rocks and other mining waste observed along the river Mtakuja in the upstream area as shown in Fig. 5. (b) is a clear indication that the activities of a gold mine are major sources of heavy metals in river Mtakuja.

a)

b)

Figure 5. (a) Acid mine drainage and (b) Tailing rocks with other mining wastes along the river Mtakuja.

Comparison of the concentration of heavy metals in fish from river Mtakuja and other rivers

The mean concentration levels of heavy metals in fish obtained from the present study from upstream areas of river Mtakuja were compared with the concentration in fish obtained from river Mara in Tanzania, Buriganga in Bangladesh and Yangtze in China. Results of the concentration levels in this work were obtained on a dry mass basis. The mean concentrations of Fe of about 429 mg/kg from this study is higher than the concentration value of 53.5reported from river Mara in Tanzania (Mohamed et al., 2016). Meanwhile, the concentration of Cr of about 18 mg/kg was higher than the concentration of 0.956 mg/kg reported from river Yangtze (Yi & Zhang, 2012), 0.3 mg/kg from river Mara and 6.33 mg/kg from Buriganga river (Ahmad et al., 2010). In addition, the concentration of Zn of about 38 mg/kg from the present work is higher than the concentration levels of 30 and 28 mg/kg reported from Yangtze and Mara rivers, respectively (Mohamed et al., 2016; Yi & Zhang, 2012). However, the concentration of Cd of 3.0 mg/kg is also higher than the Cd concentration values of about 0.5 and 1.0 mg/kg reported from Yangtze and Buriganga rivers, respectively (Yi & Zhang, 2012, Ahmad et al., 2010). In comparison, the concentration levels of Cr, Fe, Zn and Cd heavy metals in catfishes collected from river Mtakuja are significantly higher than those reported for rivers Mara, Buriganga and Yangtze. Since, fishes are good indicators of contamination in the aquatic environment (Mataba et al., 2016), the elevated concentration levels of heavy metals in fish from the river Mtakuja indicates that river Mtakuja is polluted by heavy metals.

Comparison of concentration in toxic metals in fish with Maximum Tolerable Limits (MTLs)

The concentrations of toxic metals in catfish (*clarias gariepinus*) from Mtakuja river were compared with the permissible limits recommended by Food and Agricultural Organization (FAO), World Health Organization (WHO) and European Commission (EC). The toxic metals detected in catfish include Cr, As, Cd and Pb having concentrations of 17.6, 0.2, 3.0 and 0.3 mg/kg respectively. The concentration of Cr was significant beyond the respective EC, FAO and WHO permissible limits of 0.8 mg/kg (EC 2005), 0.2 mg/kg (Joint & World Health, 2007) and 0.15 mg/kg (WHO, 2015). African Catfish feed near the bottom of the river from decaying organic matter and sediments, implying that it can certainly accumulate Cr in their tissue since Cr is known to be largely absorbed by the soil and organic matter. The concentration levels of Pb obtained from the present work were below the permissible limits of 0.5 mg/kg set by FAO/WHO (Joint & World Health, 2007). However, Pb can accumulate in sediments and other aquatic substances where catfish lives and feeds.

The concentration level measured for Cd was above the permissible level of 0.2 mg/kg as recommended by EC (EC, 2005) and 0.05 mg/kg by the WHO (2015). The high concentration values of Cr and Cd measured suggest that river Mtakuja is contaminated by heavy metals. Furthermore, high concentration levels of heavy metals in catfish (*clarias gariepinus*) can be attributed to the concentration of heavy metals that were absorbed in the sediments that were collected from the same location, since polluted sediments are known to be source of chemicals that contaminate the food chain by feeding the benthic fauna and benthopelagic feeders (Mataba et al., 2016).

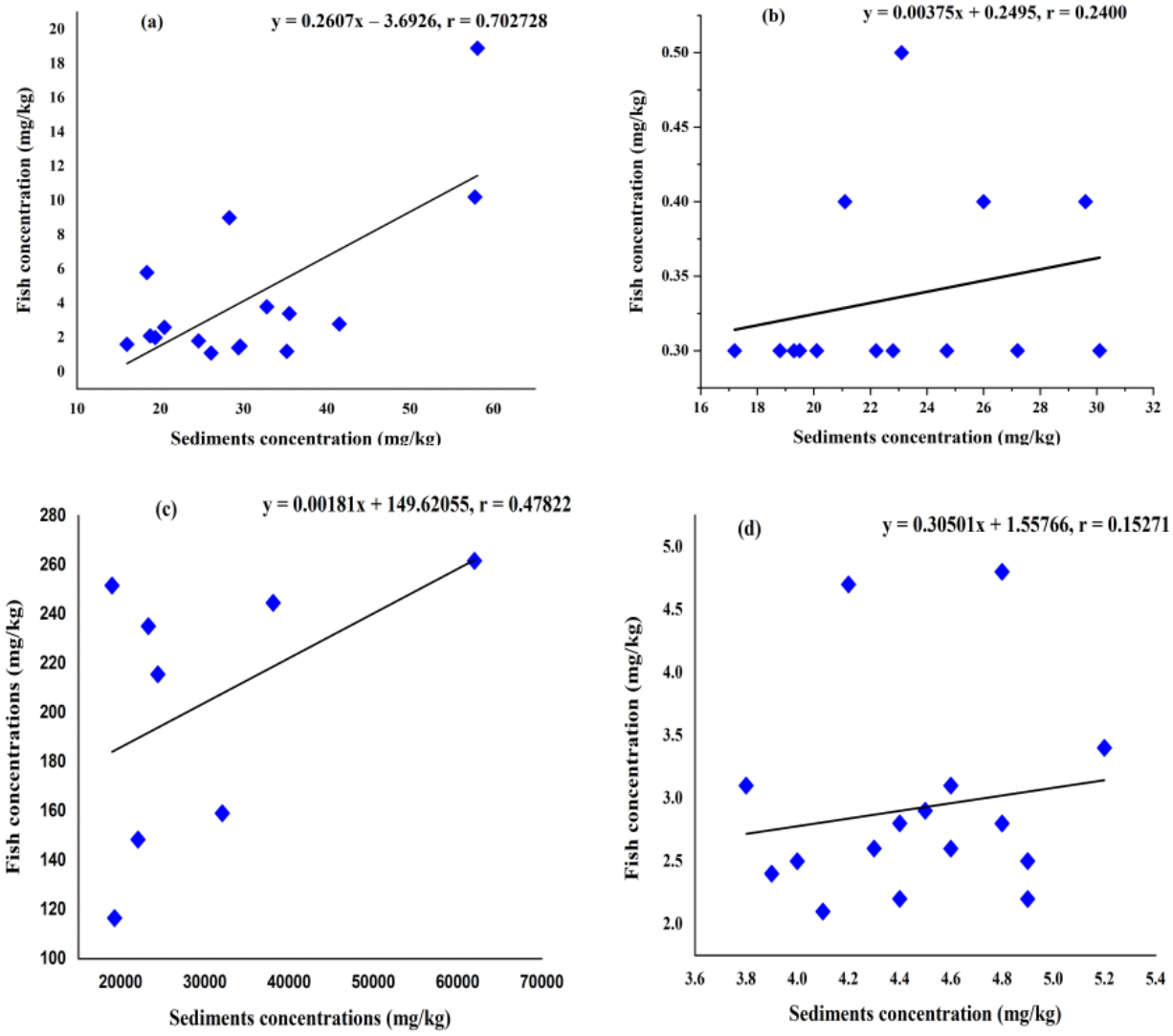

Figure 6. Correlation between concentration of heavy metals in sediments and fish for (a) Cu, (b) Pb, (c) Fe and (d) Cd.

Comparison of the concentrations of heavy metals in sediments from river Mtakuja and other rivers

The mean concentration levels of heavy metals in the sediments from river Mtakuja were compared with heavy metal concentration levels in sediments reported for rivers Tighithe and Mara in Tanzania, Buriganga in Bangladesh and Shurriver in Iran. The Concentration level of Fe of about 127627 mg/kg in river Mtakuja sediments was higher than the concentration of 10300 mg/kg from river Shur (Karbassi et al., 2008). Similar case for Cu with concentration level of about 45 mg/kg, which is higher than concentration levels of 27 mg/kg and 25 mg/kg reported for sediments from rivers Buriganga and Tighithe, respectively (Ahmad et al., 2010; Almås & Manoko, 2012). The concentration level of Cd of about 5 mg/kg was above the concentration reported in sediments from river Buriganga with concentration value of 3.31 mg/kg and river Mara of 1.53 mg/kg(Nkinda et al., 2020, Ahmad et al., 2010). Moreover, the concentration of Pb of about 22 mg/kg obtained in this study was beyond the concentration level reported in sediments from river Tighithe of 18 mg/kg (Almås & Manoko, 2012). The concentration levels of Cr of about 39 mg/kg from the present work was higher than the concentration level of 1.5 mg/kg reported in sediments of river Mara(Nkinda et al., 2020). Additionally, the concentration levels of Fe and Pb of about 127627 and 22 mg/kg obtained

from this study are significantly higher than the recommended mean world sediment concentration levels of 41000 and 19 mg/kg, respectively (Karbassi et al., 2008). Therefore, the sediment collected from river Mtakuja have Cr, Fe, Cu, Cd and Pb concentration levels that are significantly higher than recommended concentration limits.

Correlation analysis

The correlation between the concentration of the heavy metals in fish and sediments found showed the strong to weak trend given by, Cu (r = 0.70273) > Fe (r = 0.47822) > Pb (r = 0.24003) > Cd (r = 0.15271) >Cr (r = -0.17445)> Zn (r = -0.35394) >As (r = -0.42635). A positive correlation for Cu, Fe, Pb and Cd suggests possibilities of transfer for these toxic metals moving from sediment to the fish via different pathways in river Mtakuja. The negative correlation of Cr, Zn and As indicates that the sediment is not the only reason for the presence of heavy metals in fish. Therefore, the concentration levels in fish samples might also be caused by other factors that may include the presence of heavy metals in water and water hyacinth. Regression lines of the concentration of four heavy metals namely Cu, Pb, Fe and Cd for sediment and fish samples are shown in Fig.6. (a - d).

CONCLUSION

The paper reports the concentrations of heavy metals in catfish and sediments that were collected along the river Mtakuja. The results show that the river Mtakuja is polluted by heavy metals associated to both mining and domestic activities that cause discharging of wastes into Mtakuja river. In addition, runoff from agricultural lands with fertilizers, pesticides and other farming chemicals can influence the toxicity and heavy metal concentration levels in the river Mtakuja. The results also showed a positive correlation for Cu, Pb, Fe and Cd and a negative correlation for Cr, Zn and As. In conclusion, the polluted sediments can significantly increase the concentration levels of heavy metals in African Sharptooth Catfish (*clarias gariepinus*). However, the concentration levels in fish can also be influenced by the contaminated water and water hyacinth. This suggests that, there is a need for further work to refine the influences of contaminated water and water hyacinth on the heavy metals content in catfish at the river Mtakuja to discover all possible transfer mechanisms of heavy metals absorption from aquatic environment into fish.

REFERENCES

Ahmad, M. K., Islam, S., Rahman, S., Haque, M. & Islam, M. M. 2010. Heavy metals in water, sediment and some fishes of Buriganga River, Bangladesh. International J. Environmental Res, 4(2), pp. 321-332.

Almas, Å. R. & Manoko, M. L. K. 2012. Trace element concentrations in soil, sediments, and waters in the vicinity of Geita Gold Mines and North Mara Gold Mines in Northwest Tanzania. Soil and Sediment Contamination: An International Journal, 21(2), pp. 135-159. https://doi.org/10.1080/15320383.2012.649372

Baby, J., Raj, J. S., Biby, E. T., Sankarganesh, P., Jeevitha, M. V., Ajisha, S. U. & Rajan, S. S. 2010. Toxic effect of heavy metals on aquatic environment. International Journal of Biological and Chemical Sciences, 4(4), pp. 939-952. DOI: 10.4314/ijbcs.v4i4.62976

Bitala, M. F. 2008. Evaluation of heavy Metals Pollution in Soil and Plants accrued from Gold Mining activities in Geita Tanzania. MSc Thesis, University of Dar es Salaam.

Candeias, C., Ávila, P., Coehlo, P. & Teixeira, J. P. 2018. Mining activities: health impacts. Reference Module in Earth Systems and Environmental Sciences, pp. 1-21.

Casiot, C., Egal, M., Elbaz-Poulichet, F., Bruneel, O., Bancon-Montigny, C., Cordier, M.-A., Gomez, E. & Aliaume, C. 2009. Hydrological and geochemical control of metals and arsenic in a Mediterranean river contaminated by acid mine drainage (the Amous River, France); preliminary assessment of impacts on fish (Leuciscus cephalus). Applied geochemistry, 24(5), pp. 787-799. https://doi.org/10.1016/j.apgeochem.2009.01.006

Duruibe, J. O., Ogwuegbu, M. O. C. & Egwurugwu, J. N. 2007. Heavy metal pollution and human biotoxic effects. International Journal of physical sciences, 2, pp. 112-118.

Emel, J., Plisinski, J. & Rogan, J. 2014. Monitoring geomorphic and hydrologic change at mine sites using satellite imagery: The Geita Gold Mine in Tanzania. Applied Geography, 54, pp. 243-249. https://doi.org/10.1016/j.apgeog.2014.07.009

Eser, A., Kahraman, E.& Demiray, M. 2014. Comparison of atomic absorption spectroscopy and energy dispersive X-ray fluorescence spectrometer methods for chemical analysis. Asian J. Chem. 26(20), pp. 6982-6988.

European Community (EC) 2005. Commission regulation number 78/2005, Official Journal of European Union. Available at; http://data.europa.eu/eli/reg/2005/78/oj.

Jaishankar, M., Tseten, T., Anbalahan, N., Mathew, B. B. & Beeregowda, K. N. 2014. Toxicity, mechanism and health effects of some heavy metals. Interdisciplinary toxicology, 7, pp. 60-72.

Joint FAO/WHO Expert Committee on Food Additives. Meeting (67th: 2006: Rome, Italy), World Health Organization & Food and Agriculture Organization of the United Nations . (2007). Evaluation of certain food additives and contaminants: sixty-seventh report of the Joint FAO/WHO Expert Committee on Food Additives. World Health Organization. https://apps.who.int/iris/handle/10665/43592

Kadachi, A. N. & AL-Eshaikh, M. A. 2012. Limits of detection in XRF spectroscopy. X-Ray Spectrometry, 41(5), pp. 350-354. https://doi.org/10.1002/xrs.2412

Karbassi, A. R., Monavari, S. M., Nabi Bidhendi, G. R., Nouri, J. & Nematpour, K. 2008. Metal pollution assessment of sediment and water in the Shur River. Environmental monitoring and assessment, 147(1), pp. 107-116. https://doi.org/10.1007/s10661-007-0102-8

Mataba, G. R., Verhaert, V., Blust, R. & Bervoets, L. 2016. Distribution of trace elements in the aquatic ecosystem of

the Thigithe river and the fish Labeo victorianus in Tanzania and possible risks for human consumption. Science of the Total Environment, 547, pp. 48-59. https://doi.org/10.1016/j.scitotenv.2015.12.123.

Mielcarek, K., Nowakowski, P., Puscion-Jakubik, A., Gromkowska-Kepka, K. J., Soroczynska, J., Markiewicz-Żukowska, R., Naliwajko, S. K., Grabia, M., Bielecka, J. & Żmudzinska, A. 2022. Arsenic, cadmium, lead and mercury content and health risk assessment of consuming freshwater fish with elements of chemometric analysis. Food Chemistry, 379(132167), pp. 1-11. https://doi.org/10.1016/j.foodchem.2022.132167

Miri, M., Akbari, E., Amrane, A., Jafari, S. J., Eslami, H., Hoseinzadeh, E., Zarrabi, M., Salimi, J., Sayyad-Arbabi, M. & Taghavi, M. 2017. Health risk assessment of heavy metal intake due to fish consumption in the Sistan region, Iran. Environmental monitoring and assessment, 189, pp. 1-10. https://doi.org/10.1007/s10661-017-6286-7

Mohamed, N. K., Ntarisa, A. V. R., Makundi, I. N. & Kucera, J. 2016. Impact of North Mara gold mine on the element contents in fish from the river Mara, Tanzania. Journal of Radioanalytical and Nuclear Chemistry, 309, pp. 421-427. https://doi.org/10.1007/s10967-016-4756-y

Nyankweli, E. M. 2012. Foreign direct investment and poverty alleviation: the case of Bulyanhulu and Geita gold mines, Tanzania, African Studies Centre. PhD Thesis, University of Leiden.

Okereafor, U., Makhatha, M., Mekuto, L., Uche-Okereafor, N., Sebola, T. & Mavumengwana, V. 2020. Toxic metal implications on agricultural soils, plants, animals, aquatic life and human health. International journal of environmental research and public health, 17(2204), pp. 1-24. https://doi.org/10.3390/ijerph17072204

Opaluwa, O. D., Aremu, M. O., Logbo, L. O., Imagaji, J. & Eodiba, I. 2012. Assessment of heavy metals in water, fish and sediments from UKE stream, Nasarawa State, Nigeria. Current World Environment, 7(2), pp. 213-220.

Perring, L., Nicolas, M., Andrey, D., Fragnière Rime, C., Richoz-Payot, J., Dubascoux, S.& Poitevin, E. 2017. Development and validation of an ED-XRF method for the fast quantification of mineral elements in dry pet food samples. J. Food Analyt. Meth. 10(5), pp. 1469-1478. https://doi.org/10.1007/s12161-016-0695-z.

Ravisankar, R., Sivakumar, S., Chandrasekaran, A., Kanagasabapathy, K.V., Prasad, M.V.R.&Satapathy, K.K. 2015. Statistical assessment of heavy metal pollution in sediments of east coast of Tamilnadu using Energy Dispersive X-ray Fluorescence Spectroscopy (EDXRF). J. Appl. Rad. Isot. 102, pp. 42-47. https://doi.org/10.1016/j.apradiso.2015.03.018

Rousseau, R. M. 2001. Detection limit and estimate of uncertainty of analytical XRF results. Rigaku J, 18(2), pp. 33-47.

Shen, F., Mao, L., Sun, R., Du, J., Tan, Z. & Ding, M. 2019. Contamination evaluation and source identification of heavy metals in the sediments from the Lishui River Watershed, Southern China. International Journal of Environmental Research and Public Health, 16, 336. https://doi.org/10.3390/ijerph16030336

Vaiopoulou, E. & Gikas, P. 2020. Regulations for chromium emissions to the aquatic environment in Europe and elsewhere. Chemosphere, 254(126876), pp. 1-11. https://doi.org/10.1016/j.chemosphere.2020.126876

Wang, X.-N., Gu, Y.-G. & Wang, Z.-H. 2020. Fingerprint characteristics and health risks of trace metals in market fish species from a large aquaculture producer in a typical arid province in Northwestern China. Environmental technology & innovation, 19(100987), pp. 1-8. DOI: 10.1016/j.eti.2020.100987

WHO/FAO (World Health Organization/ Food and Agriculture Organization) 2015,CodexAlimentarius commission. General standards for contaminants.

Yi, Y. J. & Zhang, S. H. 2012. The relationships between fish heavy metal concentrations and fish size in the upper and middle reach of Yangtze River. Procedia Environmental Sciences, 13, pp. 1699-1707. https://doi.org/10.1016/j.proenv.2012.01.163

Bulletin of Natural Sciences Research
Vol. 13, No. 1-2, 2023, pp. 19-29.

DOI: https://doi.org/10.5937/bnsr13-41946
Original Scientific Paper

OPTIMIZATION OF THE 2P FIFTH DEGREE CONVOLUTION KERNEL IN THE SPECTRAL DOMAIN

NATAŠA SAVIĆ[1], ZORAN MILIVOJEVIĆ[2], BOJAN PRLINČEVIĆ[3]

[1]Academy of Applied Technical and Preschool Studies, Niš, Serbia
[2]University „MB“, Belgrade, Serbia
[3]Kosovo and Metohija Academy of Applied Studies, Leposavić, Serbia

ABSTRACT

The first part of the paper describes a two-parameter (2P) fifth-order interpolation kernel, *r*. After that, from the 2P kernel, the kernel components were created. By applying the Fourier transformation to each kernel component, the spectral components of the 2P kernel were obtained. The spectral characteristic of the 2P kernel, *H*, was created from the spectral components. After that, the algorithm, that optimizes the parameters of the 2P kernel so as to eliminate the ripple of the spectral characteristics, is described. The optimization was performed in such a way that the spectral characteristic developed in the Taylor series, H_T. With the condition for the elimination of the members of the Tylor series, which greatly affect the ripple of the spectral characteristic, the optimal kernel parameters (α_{opt}, β_{opt}) were determined. The second part of the paper describes an Experiment, in which the interpolation accuracy of the 2P kernel was tested. Convolution interpolation, with the 2P kernel, was performed over the signals from the Test base. The Test base is created with musical signals. By analyzing the interpolation error, which is represented by the Mean Square Error, MSE, the precision of the interpolation was determined. The results (α_{opt}, β_{opt}, MSE_{min}) are presented on tables and graphs. Detailed comparative analysis showed higher interpolation precision with the proposed 2P interpolation kernel, compared to the interpolation precision with, 1P interpolation kernel. Finally, the numerical values of the optimal kernel parameters, which are determined by the optimization algorithm proposed in this paper, were experimentally verified.

Keywords: Convolution, Interpolation, Polynomial kernel, Taylor series.

INTRODUCTION

Interpolation is the estimation of data between regular samples. It is the construction of new data based on a known set of discrete data. In digital signal processing (DSP), there is often a need to apply interpolation (audio and speech signal processing, image processing, numerical differentiation, integration, ...). A characteristic example is the spatial transformation of the image (rotation, translation,...). Most often, interpolation should be realized in real-time. The application of numerical interpolation formulas (Lagrangian, Newtonian, Gaussian, Stirling, Bessel, Chebyshev,...) requires knowledge of a large amount of data, sometimes the complete signal. For this reason, interpolation formulas are often of an impractically large order, that is, of great numerical complexity. The consequence of the high numerical complexity is an impractically long interpolation time.

One of the interpolations, which largely fulfills the criteria for working in real-time, is convolutional interpolation. Convolutional interpolation is realized by convolution between a discrete signal and a convolutional interpolation kernel. Theoretical analysis showed that the ideal convolutional interpolation kernel with time-spatial form is $r = sin(x)/x$ (Keys, 1981). The usual notation for this kernel in DSP is *sinc*. The definition range of the *sinc* kernel is $(-\infty \leq x \leq +\infty)$. This fact indicated that the *sinc* kernel is not possible to practically realize (Meijering & Unser, 2003). The solution to the problem of the infinite length of the interpolation kernel is the truncation of the kernel length. However, truncation of the *sinc* kernel causes deformations of the spectral characteristic of the *sinc* kernel. Namely, the spectral characteristic of the *sinc* kernel is a *box* characteristic (ideally flat in the pass-band and stop-band, and with an ideal slope in the transition area). The truncation length of the *sinc* kernel spectral characteristic causes a ripple in the pass-band and stop-band, and a final slope in the transition region (Dodgson, 1997). For the previously described reason, simple truncation *sinc* kernel does not give satisfactory results. For practical reasons, in DSP, the truncated *sinc* kernel is less often used. The current scientific task is to find other interpolation convolution kernels, which would realize interpolation with high precision and with high speed. Current solutions, which are proposed for use in DSP, are interpolation kernels of small lengths, which are defined on the segment $[-L, L]$, where $L \leq 8$. In addition, in order to increase the speed of interpolation, it is desirable that the kernel is presented as a mathematical function of low complexity (Milivojević et al., 2022).

Interpolation polynomial kernels are extremely relevant. The chronology of the development of the polynomial kernels is detailed in (Milivojević et al., 2022). Numerically, the least complex is the nearest-neighbor, i.e. zero-degree polynomial

*Corresponding author: bojan.prlincevic@akademijakm.edu.rs

kernel (Dodgson, 1997). The interpolation speed is extremely high. Unfortunately, the precision of the interpolation is extremely low (Rukundo & Maharaj, 2014). These features have led to a minor application of this kernel. First-degree interpolation kernel, allows linear interpolation between samples (Rifman, 1973). A quadratic, second-degree interpolation kernel is described in (Dodgson, 1997) and (Deng, 2010). A cubic, third-degree interpolation kernel, is described in (Keys, 1981). The analysis of the interpolation error, in the case of image interpolation, which is based on Taylor expansion in the spatial domain, was realized. The analysis showed that the precision of interpolation with the polynomial third-degree interpolation kernel is higher than the precision with the zero-, first- and second-degree polynomial kernels.

The paper (Keys, 1981) describes a third order polynomial kernel with an inserted parameter α. In this way, the parameterization of the kernel was performed, that is, a one-parameter (1P) kernel was formed. It is shown that by choosing the value of the parameter α, the interpolation kernel can be better adapted to the specific signal. Subsequent scientific activities went in the direction of parametrizing other kernels, with the aim of achieving higher interpolation precision. Later, in honor of the author Roberts B. Keys, the 1P interpolation kernel, described in (Keys, 1981), was named the 1P Keys kernel. The problems of reducing the ripple of the spectral characteristic were analyzed in (Meijering et al., 1999). In (Park & Schowengerdt, 1982) it was shown that the ripple of the spectral characteristic of the 1P Keys kernel is greatly reduced for the optimal parameter $\alpha = -0.5$.

The paper (Hanssen & Bamler, 1999) describes a two-parameter (α, β) third-order interpolation kernel. The construction of the 2P interpolation kernel is based on the extension of the 1P Keys kernel. For this reason, this 2P kernel is called 2P Keys kernel. The possibility of optimization of the two parameters provided greater possibilities of adaptation of the 2P kernel to specific signals. Examples of estimating the fundamental frequency, F_0, of a speech signal, by interpolation in the spectral domain, are presented in (Milivojević & Brodić, 2013) and (Milivojević et al., 2017). As a measure of the error estimate of the fundamental frequency MSE was used. The tendency to further increase the precision of the convolutional interpolation led to the construction of the 1P fifth-order interpolation kernel (Meijering et al., 1999). A further increase in the precision of the interpolation led to the construction of the 2P fifth-order interpolation kernel (Savić et al., 2021). The 2P kernel was created by expanding the 1P kernel. Examples of convolutional interpolation of audio signals with a 2P kernel are presented in (Savić et al., 2022). It is shown that the precision of interpolation is higher with interpolation with 2P compared to interpolation with 1P kernel. The interpolation error with application of Septic-convolution Kernel is analyzed in (Savić & Milivojević, 2022).

In the paper (Milivojević et al., 2022), the spectral characteristic of the 2P fifth order kernel was determined. The spectral characteristic of the 2P kernel is done as follows. It is first done by decomposing the 2P kernel into components. Then, by applying the Fourier transform to each kernel component, the spectral characteristics of each component were determined. In this way, the spectral components of the kernel are determined. Finally, taking into account all spectral components as well as the kernel parameters α and β, the spectral characteristic of the 2P kernel were determined.

In this work, the parameters (α, β) of the interpolation 2P kernel, which is described in (Savić et al., 2021), were optimized. In the first part of the paper, the analytical form of the fifth order 2P interpolation kernel is described and the components of the kernel are shown. After that, the spectral components, which are determined by applying the Fourier transformation over the kernel components, are shown (Milivojević et al., 2022). The spectral characteristic of the 2P kernel is formed by spectral components. Then the optimization of the kernel was performed. The optimization, with the criterion of eliminating the ripples of the spectral characteristic, was performed. First, the spectral characteristic was developed in the Taylor series. After that, members of the Tylor series, which dominantly affect the ripples of the spectral characteristic, were eliminated. Optimal parameters (α_{opt}, β_{opt}) were determined from the conditions of Tylor member elimination. The Experiment is described in the second part of the paper. In the Experiment, convolutional interpolation of the Test signal from the Base was performed. The Base is created from musical signals. Musical signals (tones A0, A1, ..., A7) were obtained by recording the tones interpreted on a Steinway B piano, the world-renowned piano manufacturer Steinway & Sons. The goal of the Experiment was to determine the precision of convolutional interpolation using 1P and 2P kernels, whose parameters were obtained theoretically, that is, by optimization, and whose spectral characteristics are ripple-free. The second goal of the experiment was the experimental determination of the optimal parameters of kernels in the interpolation of musical signals. Experimental determination involves minimizing the interpolation error MSE (Mean Square Error), and thus determining the optimal parameters. The results of the Experiment are presented in tabular and graphical form. At the end, a comparative analysis of the results related to the precision of interpolation was performed, and, based on it, conclusions were drawn about the efficiency of the 2P kernel.

Further organization of this paper is as follows. In Section II, the spectral characteristic of the 2P kernel is described. Section III describes the kernel parameter

optimization. In Section IV the Experiment is described. Section V is the Conclusion.

FIFTH DEGREE POLYNOMIAL CONVOLUTION KERNEL

In the paper (Meijering et al., 1999) the 1P fifth degree polynomial convolution kernel is described. The shape of the 1P kernel is, in accordance with the recommendations on the values in the nodes in the specified interval, defined in the time domain. Optimization of the kernel parameter α in the spectral domain was performed. The optimized parameter, α_{opt} = 3/64, leads to the minimization of the ripple spectral characteristic. In this way, it was achieved that the 1P kernel better approximates the spectral characteristic of the ideal *sinc* kernel. In Fig. 1 shows the time form of the shortened ideal kernel sinc, r_{sinc}. In addition, in Fig. 1 shows the time shape of the optimal 1P kernel r_{α}.

Two parameter fifth-order kernel

The paper (Savić et al., 2021) describes a new, two-parameter, polynomial interpolation convolution kernel of the fifth order (quintic-convolution kernel). The form of the 2P kernel is:

$$r(x)=\begin{cases}\left(10\alpha-10\beta-\frac{21}{16}\right)|x|^5+\\ \left(-18\alpha+18\beta+\frac{45}{16}\right)|x|^4+ & |x|\le 1\\ \left(8\alpha-8\beta-\frac{5}{2}\right)|x|^2+1,\\ \left(11\alpha-11\beta-\frac{5}{16}\right)|x|^5+\\ \left(-88\alpha+88\beta+\frac{45}{16}\right)|x|^4+\\ (270\alpha-270\beta-10)|x|^3+ & 1<|x|\le 2\\ \left(-392\alpha+392\beta+\frac{35}{2}\right)|x|^2+\\ (265\alpha-265\beta-15)|x|+\\ (-66\alpha+66\beta+5),\\ \alpha|x|^5+(-14\alpha+3\beta)|x|^4+\\ (78\alpha-30\beta)|x|^3+\\ (-216\alpha+112\beta)|x|^2+ & 2<|x|\le 3\\ (297\alpha-185\beta)|x|+\\ (-162\alpha+114\beta),\\ \beta|x|^5-19\beta|x|^4+144\beta|x|^3- & 3<|x|\le 4\\ 544\beta|x|^2+1024\beta|x|-768\beta,\\ 0, & |x|>4\end{cases}, \quad (1)$$

where α and β are kernel parameters. The 2P kernel can be presented in the form (Milivojević et al., 2022):

$$r(x)=r_0(x)+\alpha r_1(x)+\beta r_2(x), \quad (2)$$

where r_0, r_1 and r_2 are kernel components:

$$r_0(x)=\begin{cases}\frac{-21}{16}|x|^5+\frac{45}{16}|x|^4-\\ -\frac{5}{2}|x|^2+1 & , \quad |x|\le 1\\ \frac{-5}{16}|x|^5+\frac{45}{16}|x|^4-10|x|^3+\\ \frac{35}{2}|x|^2-15|x|+5 & , \quad 1<|x|\le 2\\ 0 & , \quad |x|>2\end{cases}, \quad (3)$$

$$r_1(x)=\begin{cases}10|x|^5-18|x|^4+8|x|^2, & 0<|x|\le 1\\ 11|x|^5-88|x|^4+270|x|^3-392|x|^2+\\ +265|x|-66, & 1<|x|\le 2\\ |x|^5-14|x|^4+78|x|^3-216|x|^2+\\ 297|x|-162, & 2<|x|\le 3\\ 0; & |x|>3\end{cases}, \quad (4)$$

and

$$r_2(x)=\begin{cases}-10|x|^5+18|x|^4-8|x|^2 & 0\le|x|\le 1\\ -11|x|^5+88|x|^4-270|x|^3+ & 1<|x|\le 2\\ +392|x|^2-265|x|+66\\ 3|x|^4-30|x|^3+112|x|^2- & 2<|x|\le 3\\ -185|x|+114\\ |x|^5-19|x|^4+144|x|^3- & 3<|x|\le 4\\ -544|x|^2+1024|x|-768\\ 0 & |x|>4\end{cases}. \quad (5)$$

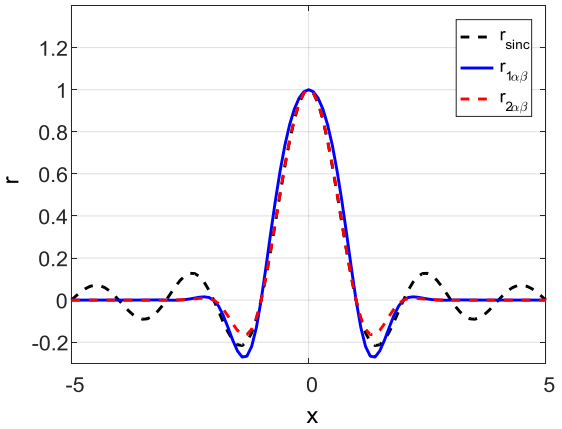

Figure 1. Interpolation 2P kernel: time domain, r_{sinc} - ideal *sinc* kernel, $r_{1\alpha\beta}$ - (α = 0.1, β = -0.01), $r_{2\alpha\beta}$ - (α = 0.2, β = 0.01).

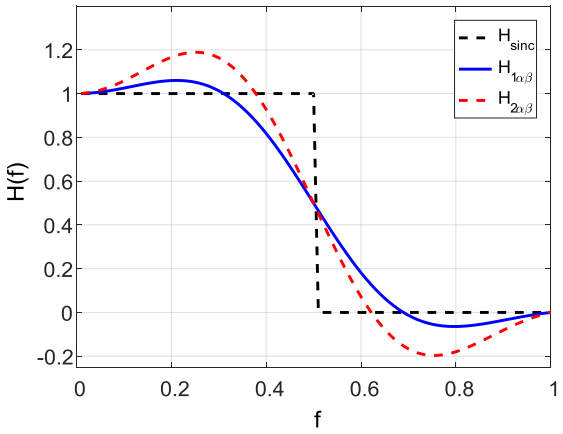

Figure 2. Interpolation 2P kernel: spectral domain , H_{sinc} - *box*, $H_{1\alpha\beta}$ - (α = 0.1, β = -0.01), $H_{2\alpha\beta}$ - (α = 0.2, β = 0.01).

The effect of the kernel parameters α and β on time shape kernels is shown in Fig. 1: a) $r_{1\alpha\beta}$ (α = 0.1, β = -0.01) and b) $r_{2\alpha\beta}$ (α = 0.2, β = 0.01). r_{sync} is a time shape of the truncate *sinc* kernel. The spectral characteristics are shown in Fig. 2.: a) $H_{1\alpha\beta}$ (α = 0.1, β = -0.01) and b) $H_{2\alpha\beta}$ (α = 0.2, β = 0.01). H_{sinc} is the spectral *box* characteristic of the ideal kernel.

Spectral characteristic of the 2P kernel

The spectral characteristic of the 2P polynomial convolutional interpolation fifth order kernel, *r*, is presented in (Milivojević et al., 2022). The 2P kernel is obtained by applying a Fourier transform over the time shape of the kernel Eq. (1). More precisely, the Fourier transform is applied over each kernel component r_0, r_1 and r_2 Eq. (3 - 5). In this way, the spectral components of the 2P kernel H_0, H_1 and H_2, were calculated. The spectral components of the 2P kernel are:

$$H_0 = \frac{15\sin[f\pi]}{32f^6\pi^6}\begin{pmatrix}-2f\pi(17\cos[f\pi]+\cos[3f\pi])+\\ 21\sin[f\pi]+5\sin[3f\pi]\end{pmatrix}, \quad (6)$$

$$H_1 = \frac{3\sin[2f\pi]}{2f^6\pi^6}\begin{pmatrix}66f\pi+50\sin[2f\pi]-5\sin[4f\pi]+\\ 2f\pi(26\cos[2f\pi]+\cos[4f\pi])\end{pmatrix}, \quad (7)$$

and

$$H_2 = \frac{\sin[2f\pi]}{2f^6\pi^6}\begin{pmatrix}-2f\pi(87+4f^2\pi^2+72\cos[2f\pi])\\ -150\sin[2f\pi]+15\sin[4f\pi]-15\sin[6f\pi]\\ +2f\pi((21-8f^2\pi^2)\cos[4f\pi]+3\cos[6f\pi])\end{pmatrix}. \quad (8)$$

Finally, the spectral characteristic is:

$$H(f)=H_0(f)+\alpha H_1(f)+\beta H_2(f). \quad (9)$$

OPTIMIZATION OF THE 2P KERNEL

By changing the value of the parameters of the 2P kernel (α, β), its time-spatial shape (Eq. (1)) as well as the shape of the spectral characteristic (Eq. (9)) are affected. In this way, it is achieved that the spectral characteristic is more similar to the spectral characteristic of the ideal, *sinc* kernel (box function). Therefore, the precision of convolutional interpolation with 2P kernel increases.

In the further part of this paper, applying the criterion of reducing the ripple of the spectral characteristic, the optimization of kernel parameters is described (Fig. 1). The optimization process was carried out in the following steps. Over the spectral components H_0, H_1 and H_2, (Eq. (6 - 8)) Taylor expansion was applied.

In this way, the Taylor spectral components H_{T0}, H_{T1} and H_{T2}, were obtained:

$$H_{T0}(f)=1-\frac{3f^2\pi^2}{14}-\frac{f^4\pi^4}{105}+\frac{89f^6\pi^6}{10395}-\frac{458f^8\pi^8}{315315}+O\left((f\pi)^{10}\right), \quad (10)$$

$$H_{T1}(f)=\frac{32f^2\pi^2}{7}-\frac{352f^4\pi^4}{105}+\frac{2144f^6\pi^6}{3465}+\frac{75904f^8\pi^8}{945945}+O\left((f\pi)^{10}\right), \quad (11)$$

and

$$H_{T2}(f)=-\frac{176f^2\pi^2}{35}+\frac{1936f^4\pi^4}{315}-\frac{14512f^6\pi^6}{2475}+\frac{22309568f^8\pi^8}{4729725}+O\left((f\pi)^{10}\right), \quad (12)$$

respectively.

The spectral characteristic of the 2P kernel, composed of Taylor components, is

$$\begin{aligned}H_T(f)&=H_{T0}(f)+\alpha H_{T1}(f)+\beta H_{T2}(f)=\\ &1-\frac{1}{70}(15-320\alpha+352\beta)(f\pi)^2-\\ &\frac{1}{315}(3+1056\alpha-1936\beta)(f\pi)^4+\\ &\frac{1}{51975}(445+32160\alpha-304752\beta)(f\pi)^6+\\ &\frac{1}{4729725}(-6870+379520\alpha+22309568\beta)(f\pi)^8+\\ &O\left((f\pi)^{10}\right)\end{aligned}. \quad (13)$$

The second and third elements in the Taylor series (Eq. (13)) have a dominant influence on the ripple of the spectral characteristics (Fig. 2.). For this reason, the second and third terms should be eliminated in the optimization process, so that the corresponding coefficients should be equal to zero:

$$\begin{cases}15-320\alpha+352\beta=0\\ 3+1056\alpha-1936\beta=0\end{cases}. \quad (14)$$

By solving the system of equations (Eq. (14)), the values of the optimal parameters of the 2P kernel were calculated

$$\alpha_{opt} = \frac{171}{1408} \approx 0.121, \quad \beta_{opt} = \frac{525}{7744} \approx 0.068.$$

In Fig. 3, in addition to the time shape of the shortened ideal kernel *sinc*, (r_{sinc}), and the time shape of the optimal 1P kernel (r_α), the time shape of the optimal 2P kernel $r_{\alpha\beta}$ is shown. It can be seen that the time shape of the 2P kernel is more similar to the *sinc* kernel, compared to the shape of the 1P kernel.

In Fig. 4 spectral characteristics: a) ideal *sinc* kernel (H_{sinc} - box characteristic), b) optimal 1P kernel (H_α, α_{opt} = 3/64) and c) optimal 2P kernel ($H_{\alpha\beta}$, α_{opt} = 171 / 1408, β_{opt} = 525/7744), are shown. It can be seen that the spectral characteristics of 1P and 2P kernels are smooth, that is, ripples are eliminated, which was the optimization criterion. In addition, the spectral characteristic of the 2P kernel better approximates the *box* characteristic of the ideal kernel, compared to the spectral characteristic of the 1P kernel.

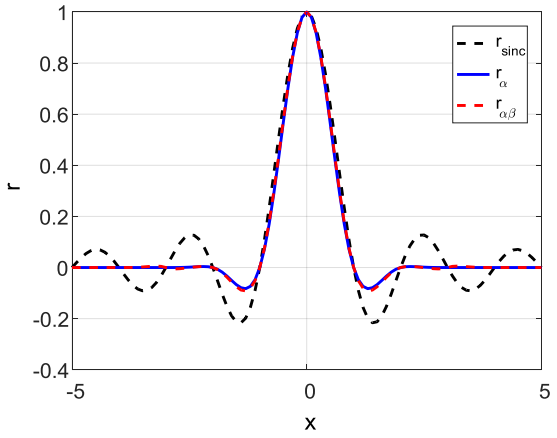

Figure 3. Interpolation kernel (time domain): a) r_{sinc} - ideal kernel b) r_α - optimal 1P kernel (α_{opt} = 3 / 64) and c) $r_{\alpha\beta}$ - optimal 2P (α_{opt} = 171 / 1408, β_{opt} = 525 / 7744).

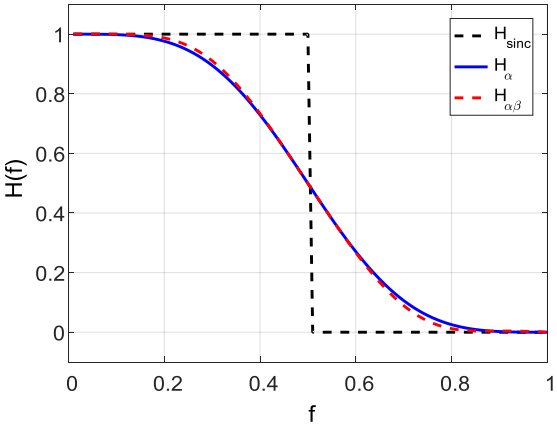

Figure 4. Spectral characteristic of interpolation kernel: a) H_{sinc} - ideal kernel b) H_α - optimal 1P kernel (α_{opt} = 3 / 64) and c) $H_{\alpha\beta}$ - optimal 2P (α_{opt} = 171 / 1408, β_{opt} = 525 / 7744).

In Fig. 4 spectral characteristics: a) ideal *sinc* kernel (H_{sinc} - box characteristic), b) optimal 1P kernel (H_α, α_{opt} = 3 / 64) and c) optimal 2P kernel ($H_{\alpha\beta}$, α_{opt} = 171 / 1408, β_{opt} = 525 / 7744) , are shown. It can be seen that the spectral characteristics of 1P and 2P kernels are smooth, that is, ripples are eliminated, which was the optimization criterion. In addition, the spectral characteristic of the 2P kernel better approximates the *box* characteristic of the ideal kernel, compared to the spectral characteristic of the 1P kernel.

EXPERIMENTAL RESULTS AND ANALYSIS

Experiment

The optimal parameter of the fifth order 1P kernel was calculated in (Meijering et al., 1999) (α_{opt} = 3 / 64 = 0.046). In this paper the optimal parameters of the 2P kernel were determined (α_{opt} = 171 / 1408 = 0.121 and β_{opt} = 525 / 7744 = 0.068). Using the Experiment, a comparative analysis of the accuracy of convolutional interpolation with 1P kernel and 2P kernel was analyzed. The interpolation is performed on the Test signals from the Base. The Base is created from music signals. As a measure of interpolation precision, the Root Mean Square error (MSE) was applied. First, convolutional interpolation with optimal 1P and 2P interpolation kernels was performed. By comparative analysis of interpolation precision, the efficiency of the kernels, which were optimized in relation to minimizing the ripples spectral characteristic, was determined. After that, in the second part of the Experiment, the interpolation of musical signals in a wide range for the kernel parameters (α = -1, ..., 0.5, β = -1, ..., 1), was performed. By minimizing the MSE interpolation error, the optimal parameters of the kernels are determined (1P kernel $\Rightarrow$ $\alpha_{opt} = \arg\min_{\alpha}(\mathrm{MSE}(\alpha))$ Fig. 7, and 2P kernel $\Rightarrow$ $(\alpha_{opt}, \beta_{opt}) = \arg\min_{\alpha,\beta}(\mathrm{MSE}(\alpha,\beta))$ Fig. 8. The results are presented using tables. At the end, a comparative analysis of the results was performed and the higher precision of the 2P compared to the 1P kernel was determined.

Base

For the purposes of the Experiment, the Base, which is composed of musical signals. Musical tones A0 - A7 are interpreted on a Steinway B piano, the world-renowned piano manufacturer Steinway & Sons. The recording was made at the University of Iowa and is part of the RWC Music Database (Goto et al., 2003). Recording was done with *Fs* = 44100 Hz and 16 bps. Musical Test signals are shown in: a) Fig. 5 (time domain) and b) Fig. 6 (spectral domain).

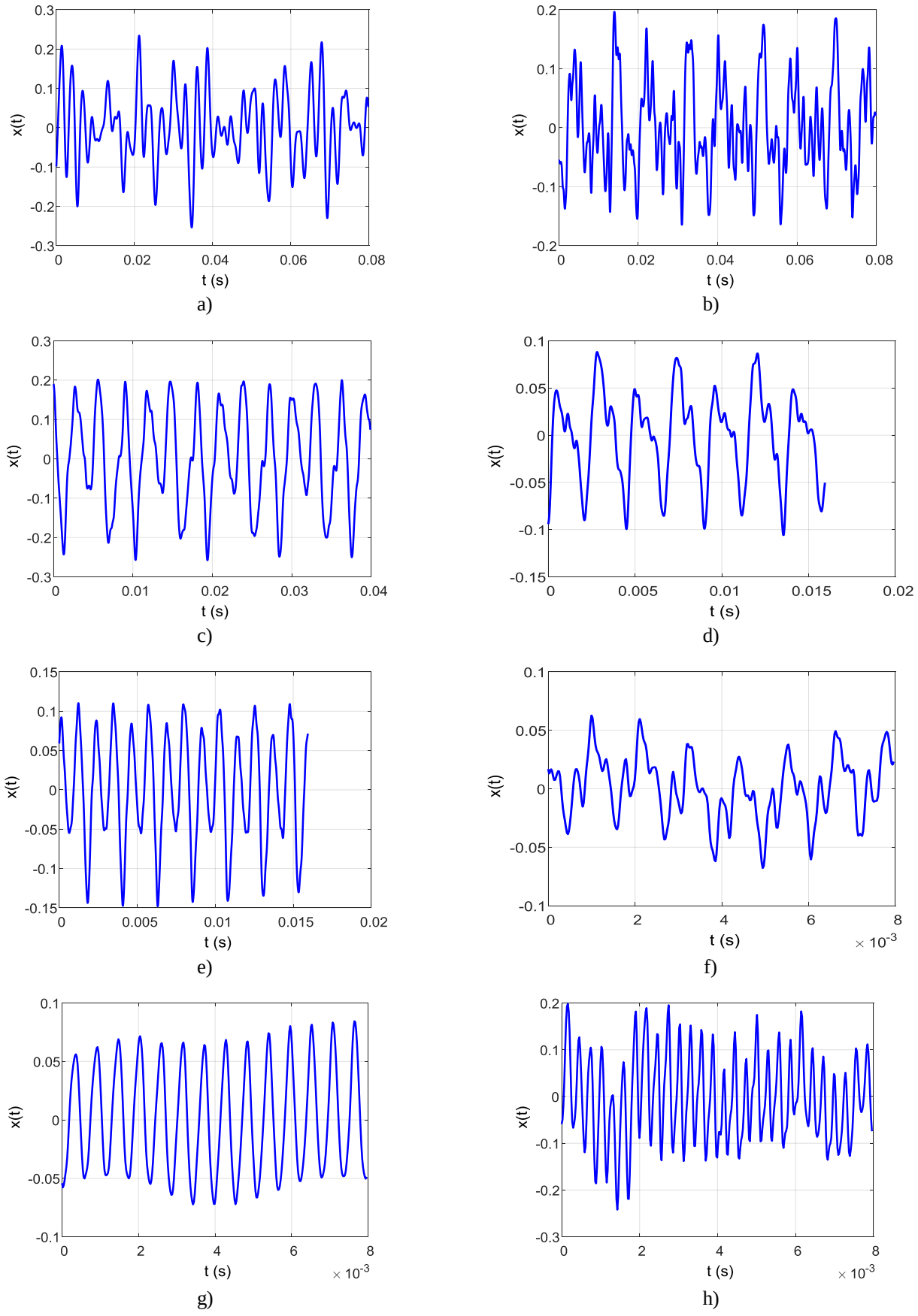

Figure 5. Musical Test signals in the time domain: a) A0, b) A1, c) A2, d) A3, e) A4, f) A5, g) A6 and h) A7.

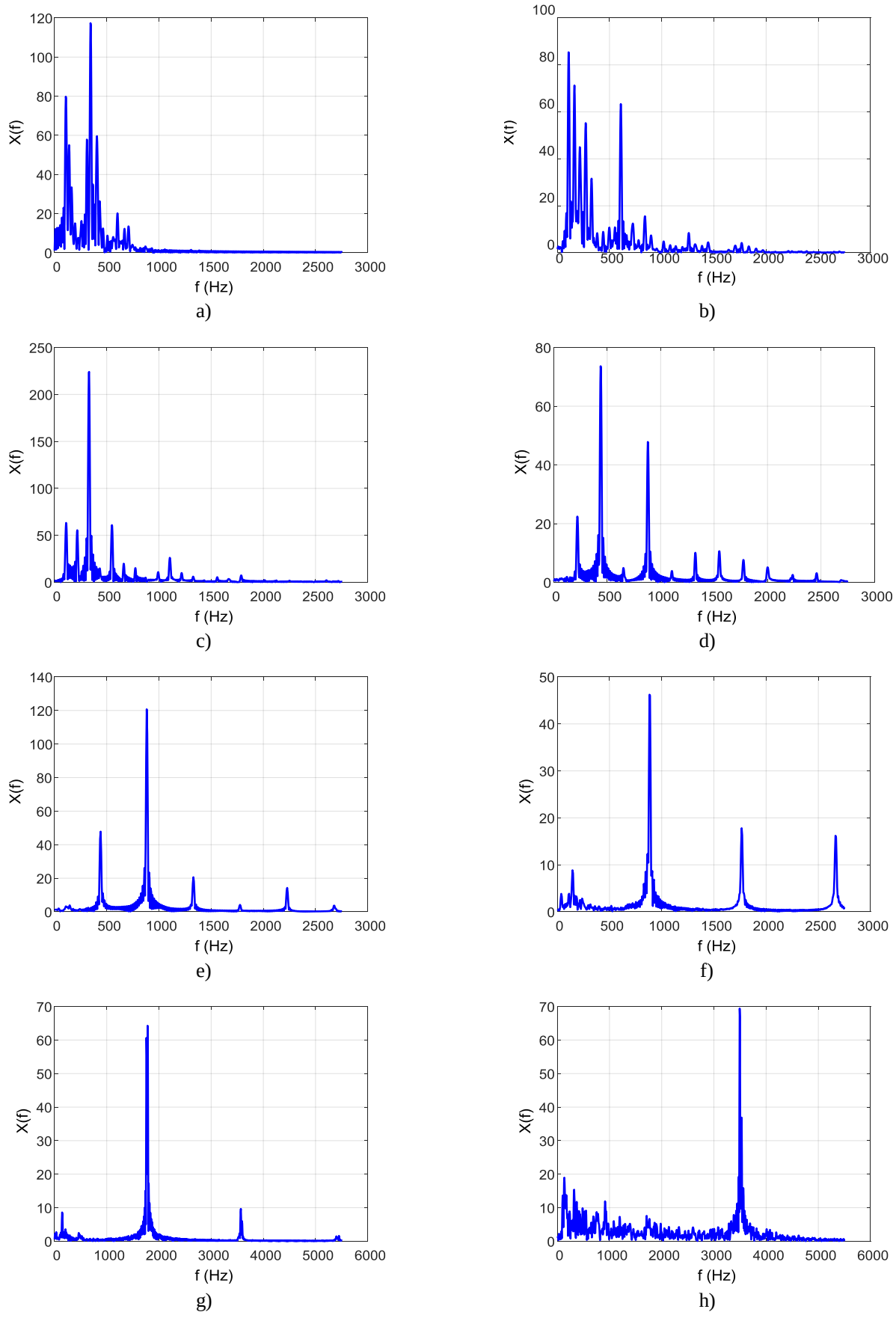

Figure 6. Musical test signals in the spectral domain: a) A0, b) A1, c) A2, d) A3, e) A4, f) A5, g) A6 and h) A7.

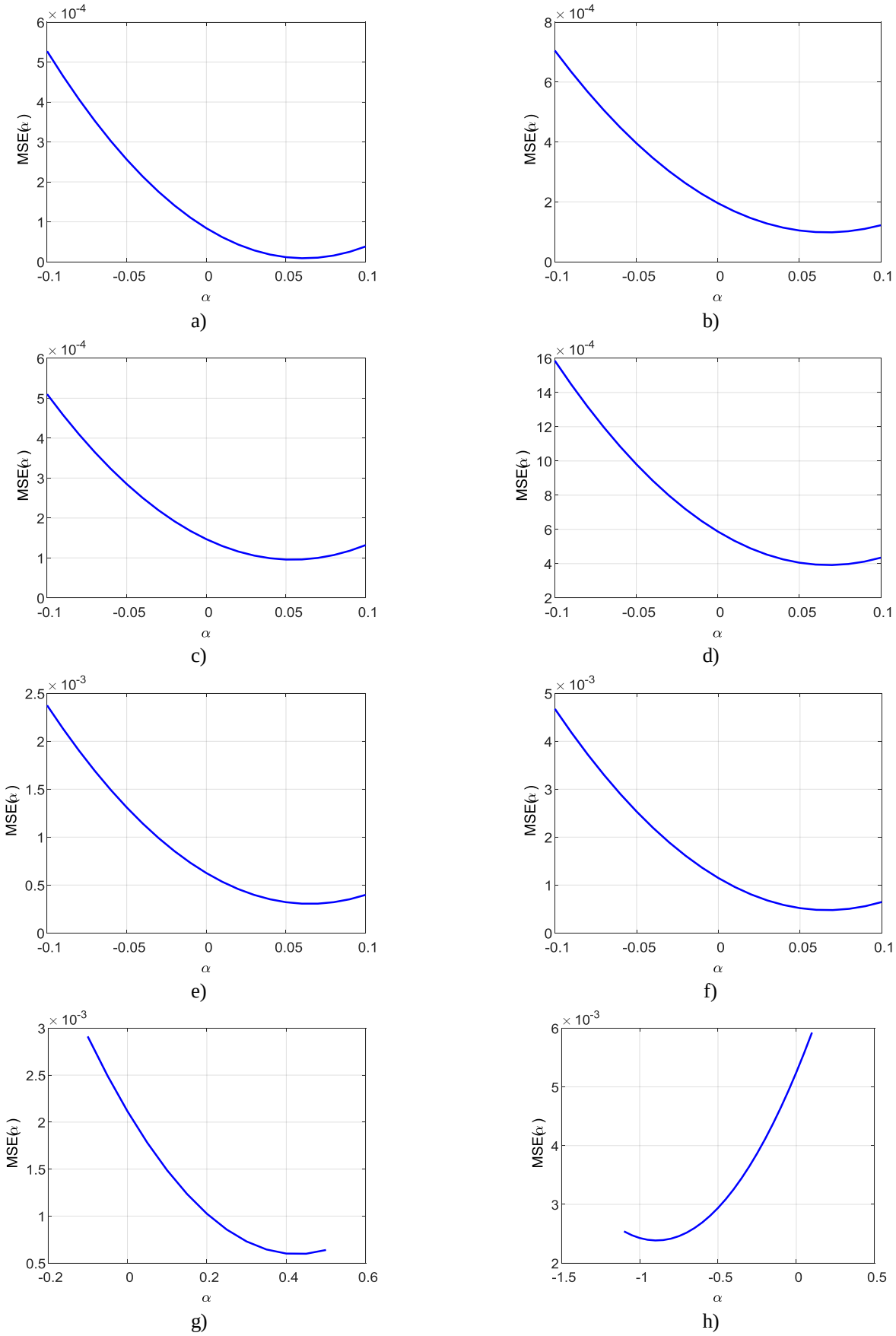

Figure 7. MSE(α) for 1P kernel for musical tones: a) A0, b) A1, c) A2, d) A3, e) A4, f) A5, g) A6 and h) A7.

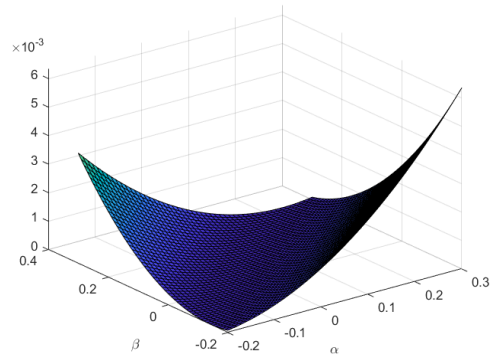

a)

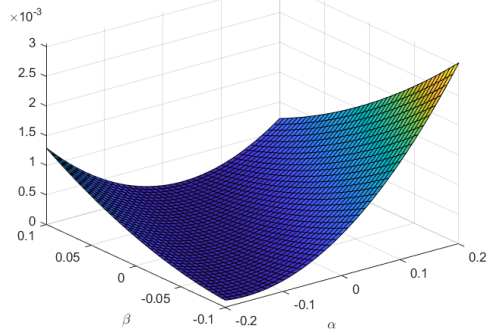

b)

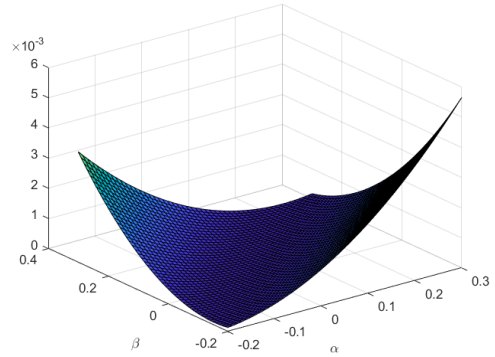

c)

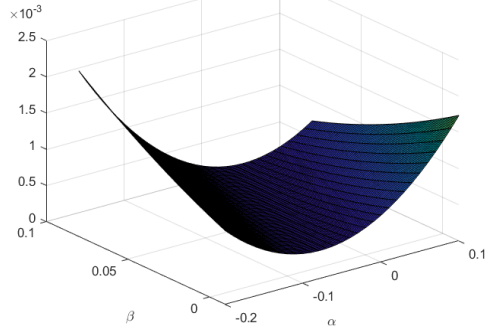

d)

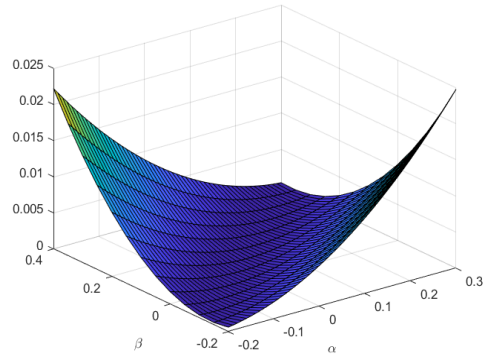

e)

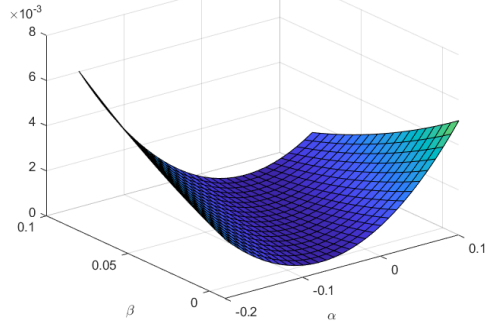

f)

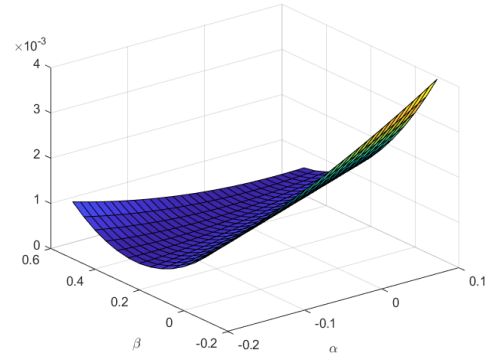

g)

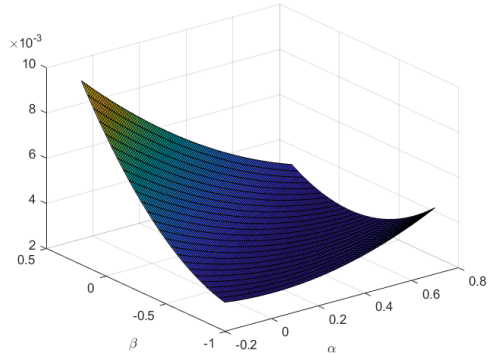

h)

Figure 8. MSE(*α, β*) for 2P kernel for musical tones: a) A0, b) A1, c) A2, d) A3, e) A4, f) A5, g) A6 and h) A7.

Results

The interpolation errors MSE of musical Test signals, in convolutional interpolation with optimal 1P and 2P fifth-order kernels, are shown in Table 1. The minimum MSE and optimal parameters α_{opt}, for the 1P kernel are shown in Table 2. The minimum MSE and the optimal parameters α_{opt} and β_{opt} for the 2P kernel are shown in Table 3. The interpolation errors are shown by graphs for: a) 1P kernel (Fig. 7, MSE(α)) and 2P kernel (Fig. 8, MSE(α, β)).

Table 1. Interpolation errors MSE in with optimal 1P and 2P interpolation kernels.

Tone	MSE	
	1P	**2P**
A0	$1.3052\ 10^{-5}$	$1.0012 \cdot 10^{-5}$
A1	$1.0686\ 10^{-4}$	$1.0283\ 10^{-4}$
A2	$9.6588\ 10^{-5}$	$9.5695\ 10^{-5}$
A3	$4.1070 \cdot 10^{-4}$	$4.0181\ 10^{-4}$
A4	$3.2884 \cdot 10^{-4}$	$3.1281\ 10^{-4}$
A5	$5.3470 \cdot 10^{-4}$	$4.9720\ 10^{-4}$
A6	$1.8008 \cdot 10^{-3}$	$1.7859 \cdot 10^{-3}$
A7	$5.5589 \cdot 10^{-3}$	$5.5555 \cdot 10^{-3}$
	$\overline{MSE_{\alpha}}$	$\overline{MSE_{\alpha\beta}}$
	0.0011	0.0010

Table 2. Minimum MSE and optimal parameters α_{opt}, for the 1P kernel.

tone	α_{opt}	MSE_{α}
A0	0.0600	$8.8281\ 10^{-6}$
A1	0.0700	$9.8313\ 10^{-5}$
A2	0.0500	$9.5954\ 10^{-5}$
A3	0.0700	$3.9186\ 10^{-4}$
A4	0.0600	$3.0580\ 10^{-4}$
A5	0.0700	$4.7789\ 10^{-4}$
A6	0.4500	$5.9965\ 10^{-4}$
A7	-0.9000	0.0024
	$\overline{\alpha_{opt}}$	$\overline{MSE_{\alpha}}$
	-0.0087	$5.4729\ 10^{-4}$

Table 3. Minimum MSE and the optimal parameters α_{opt} and β_{opt} for the 2P kernel.

Tone	α_{opt}	β_{opt}	$MSE_{\alpha\beta}$
A0	0.2800	0.2200	$7.9855\ 10^{-6}$
A1	-0.0550	-0.1200	$9.7994\ 10^{-5}$
A2	0.2000	0.1400	$9.5462\ 10^{-5}$
A3	-0.0020	-0.0700	$3.9151\ 10^{-4}$
A4	0.3500	0.2800	$2.9661\ 10^{-4}$
A5	0.0750	0.0100	$4.7624 \cdot 10^{-4}$
A6	0.2500	-0.1700	$5.8914 \cdot 10^{-4}$
A7	-0.1000	0.7900	0.0023
	$\overline{\alpha_{opt}}$	$\overline{\beta_{opt}}$	$\overline{MSE_{\alpha\beta}}$
	0.1247	0.135	$5.3187 \cdot 10^{-4}$

Analysis of results

In accordance with the results shown in Table 1 (1P and 2P kernels with optimal parameters), it is concluded that MSE, when applying 2P kernel compared to 1P Keys kernel $\overline{MSE_{\alpha}}$ / $\overline{MSE_{\alpha\beta}}$ = 0.0011/0.0010 = 1.1 times smaller.

Based on the experimental results shown in Table 2 and Table 3, by comparative analysis of MSE, it is concluded that: a) MSE, when applying 2P kernel compared to 1P kernel $\overline{MSE_{\alpha}}$ / $\overline{MSE_{\alpha\beta}}$ = $5.4729\ 10^{-4}$ / $5.3187 \cdot 10^{-4}$ = 1.029 times smaller. b) the range of optimal values of the parameter of the 1P kernel (Table 2) $\alpha_{opt} \in [-0.9 \div 0.45]$ and that the mean value $\overline{\alpha_{opt}}$ = - 0.0087. c) range of optimal parameter values of the 2P kernel (Table 3) $\alpha_{opt} \in [-0.1 \div 0.35]$ and $\beta_{opt} \in [-0.17 \div 0.79]$ and mean value $\overline{\alpha_{opt}}$ = 0.1247 and $\overline{\beta_{opt}}$ = 0.135. d) the estimation error of the parameters α is $\Delta\alpha = |\alpha_{opt} - \overline{\alpha_{opt}}| = |0.1214 - 0.1247| = 0.0033$, where the theoretical α_{opt} = 171 / 1408 =0.1214. e) the estimation error of the parameters β is $\Delta\beta = |\beta_{opt} - \overline{\beta_{opt}}| = |0.0678 - 0.135| = 0.0672$, where the theoretical β_{opt} = 0.0678. The total parameter estimation error for musical tones is $E_T = \sqrt{\Delta_{\alpha}^2 + \Delta_{\beta}^2}$ = 0.0045. In accordance with the performed comparative analysis of MSE for 1P and 2P interpolation kernels of the fifth order, it is concluded that convolutional interpolation with 2P kernel is more accurate compared to interpolation with 1P kernel.

CONCLUSION

The paper presents an algorithm for optimizing the parameters of the 2P fifth order interpolation kernel. Parameter optimization was performed in the spectral domain by minimizing the ripple of the spectral characteristic. First, the spectral characteristic was developed in the Taylor series, and, after that, the members of the Taylor series that had a great effect on increasing the ripple of the spectral characteristic, were eliminated. From the conditions of elimination of the dominant members of the Taylor series, the optimal values of the parameters of the 2P kernel (α_{opt} = 0.121, β_{opt} = 0.068), were determined. Verification of the accuracy of the 2P kernel when interpolating musical signals (tones A0, A1, ..., A7) was performed experimentally. The interpolation accuracy is expressed through the MSE interpolation error. Detailed comparative analysis showed that the 2P kernel, with theoretically determined optimal parameters, has a higher interpolation accuracy compared to the 1P kernel 1.1 times. In addition, comparative analysis showed that the 2P kernel, with experimentally determined optimal parameters, has a higher interpolation accuracy compared to the 1P kernel 1,029 times. Based on the presented results, it is concluded that the 2P fifth-order kernel is superior to the 1P kernel, and that the

interpolation error is smaller. The 2P fifth-order kernel with optimal parameters α_{opt} and β_{opt}, compared to the ideal *sinc* kernel, has less numerical complexity, and therefore, it is suitable for implementation in convolutional interpolations for operation in real-time systems.

REFERENCES

Deng, T.-B. 2010. Frequency-domain weighted-least-squares design of quadratic interpolators. IET Signal Processing, 4(1), 102. https://doi.org/10.1049/iet-spr.2008.0125

Dodgson, N. A. 1997. Quadratic interpolation for Image Resampling. IEEE Transactions on Image Processing, 6(9), pp. 1322-1326. https://doi.org/10.1109/83.623195

Goto, M., Hashiguchi, H., Nishimura, T., Oka, R. 2003. RWC Music Database:Music Genre Database and Musical Instrument Sound Database. Proceedings of the 4th International Conference on Music Information Retrieval, pp. 229-230.

Keys, R. 1981. Cubic convolution interpolation for digital image processing. IEEE Transactions on Acoustics, Speech, and Signal Processing, 29(6), pp. 1153-1160. https://doi.org/10.1109/tassp.1981.1163711

Meijering, E. H. W., Zuiderveld, K. J., Viergever, M. A. 1999. Image reconstruction by convolution with symmetrical piecewise nth-order polynomial kernels. IEEE Transactions on Image Processing, 8(2), pp. 192-201. https://doi.org/10.1109/83.743854

Meijering, E., Unser, M. 2003. A note on cubic convolution interpolation. IEEE Transactions on Image Processing, 12(4), pp. 477-479. https://doi.org/10.1109/tip.2003.811493

Milivojević, Z. N., Brodić, D. 2013. Estimation of the fundamental frequency of the speech signal compressed by MP3 algorithm. Archives of Acoustics, 38(3), pp. 363-373. https://doi.org/10.2478/aoa-2013-0043

Milivojević, Z., Savić, N., Brodić, D. 2017. Three-parametric cubic interpolation for estimating the fundamental frequency of the speech signal. Computing and Informatics, 36(2), pp. 449-469. https://doi.org/10.4149/cai_2017_2_449

Milivojević, Z., Savić, N., Prlinčević, B. 2022. Spectral characteristics of two parameter fifth degree polynomial convolution kernel. Bulletin of Natural Sciences Research, 12(1), pp. 15-20. https://doi.org/10.5937/bnsr12-38771

Park, S. K., Schowengerdt, R. A. 1983. Image reconstruction by parametric cubic convolution. Computer Vision, Graphics, and Image Processing, 23(3), pp. 258-272. https://doi.org/10.1016/0734-189x(83)90026-9

Rukundo, O., Maharaj, B. T. 2015. Optimization of image interpolation based on nearest neighbour algorithm. Proceedings of the 9th International Conference on Computer Vision Theory and Applications, pp. 641-647. https://doi.org/10.5220/0004742506410647

Savić, N., Milivojević, Z. 2021. Optimization of Parameters of the 2P Fifth Degree Interpolation Kernel for Interpolation of Audio Signals. 21st International Symposium INFOTEH-JAHORINA, pp. 207-210.

Savić, N., Milivojević, Z., Prlinčević, B. 2021. Development of the 2P fifth-degree interpolation convolutional kernel. International Journal of Innovative Research in Advanced Engineering, 8(11), pp. 306-311. https://doi.org/10.26562/ijirae.2021.v0811.003

Savić, N., Milivojević, Z, Prlinčević, B., Kostić, D. 2022. Septic-convolution Kernel - Comparative Analysis of the Interpolation Error, 2022 International Conference on Development and Application Systems (DAS). https://ieeexplore.ieee.org/document/9786191/authors#authors

Bulletin of Natural Sciences Research
Vol. 13, No. 1-2, 2023, pp. 30-34.

DOI:https://doi.org/10.5937/bnsr13-44582
Original Scientific Paper

ON THE SECOND ORDER STATISTICS OF THE RATIO OF TWO FISHER-SNEDECOR RANDOM VARIABLES AND ITS APPLICATION TO INTERFERENCE LIMITED COMMUNICATIONS

ČASLAV STEFANOVIĆ[1], DANIJEL ĐOŠIĆ[1,⋆], STEFAN PANIĆ[1]

[1]Faculty of Sciences and Mathematics, University of Priština in Kosovska Mitrovica, Kosovska Mitrovica, Serbia

ABSTRACT

The paper investigates the higher order statistics of the ratio of two Fisher-Snedecor F (FS-F) random variables (RVs) and its application to wireless communications in the presence of co-channel interference. Namely, the work provides novel expressions for probability density function (PDF), cumulative density function (CDF), level crossing rate (LCR) and average fade duration (AFD) of the ratio of two FS-F RVs. Numerical examples of the analytically derived statistical measures in terms of FS-F multi-path and shadowing parameters are shown and examined. Moreover, the impact of the number of interferes on the considered measures are further presented and examined.

Keywords: 5G, Fisher-Snedecor F (FS-F) distribution, Second order statistics.

INTRODUCTION

A Fisher-Snedecor F (FS-F) distribution has been recently proposed as a tractable and experimentally tested composite fading model that can be efficiently applied for 5G and beyond 5G wireless communication systems (WCS) (Yao et al., 2021; Zhang et al., 2019; Makarfi et al., 2020).

Namely, the FS-F distribution has been introduced in (Yoo et al., 2017). In (Badarneh et al., 2018a), authors examined the sum of FS-F RVs and its application to maximal-ratio-combining (MRC) while selection combining (SC) and switch-and-stay combining (SSC) techniques over FS-F fading channels are considered in (Al-Hmood & Al-Raweshidy, 2020; Cheng et al., 2021), respectively. Dual-hop relay-assisted WCS over FS-F channels is examined in (Zhang et al., 2020). Physical layer security over FS-F distribution is further investigated in (Kong & Kaddoum, 2018). The first order statistics (FO-S) of cascaded N-FS-F distribution is considered in (Badarneh et al., 2018b) while the FO-S of the ratio of FS-F distribution is further considered in (Badarneh et al., 2020; Du et al., 2019). The first order performance analysis of communication systems in interference limited environments where the transmission signal as well as interference signal are modeled with FS-F distribution are given in (Alshawaqfeh et al., 2022). The second order statistics (SO-S) in terms of level crossing rate (LCR) and average fade duration (AFD) of FS-F distribution are provided in (Yoo et al., 2019) while the LCR and AFD of the product of two FS-F RVs are provided in (Stefanovic et al., 2021a). SO-S of N-FS-F fading model and their application to multihop communications are provided in (Stefanovic et al., 2021b, 2022b). Moreover, SO-S over cascaded N-Gamma-gamma (N-GG) fading channels are investigated in (Stefanović et al., 2021). The SO-S of SC combining systems with the co-channel interference over various fading channels are investigated in (Hadzi-Velkov, 2006, 2007a,b; Stefanović et al., 2012). Furthermore, SO-S of Unmanned Aerial vehicle (UAV)-to-ground, mobile-to-mobile (M2M), vehicle-to-infrastructure (V2I) and macro-diversity communications in interference limited scenarios have been investigated, respectively in (Stefanovic et al., 2022a; Đošić et al., 2022; Milosevic et al., 2018b,a; Stefanovic et al., 2018; Suljović et al., 2020).

Since the co-channel interference (CCI) is one of the major factors that can negatively impact the system performances, this paper examines LCR and AFD of ratio of two FS-F RVs and its application to the interference limited communication scenarios. To the best of the author's knowledge there is no paper that investigates SO-S of the ratio of the FS-F F RVs.

SYSTEM MODEL

The ratio of two independent Fisher-Snedecor F (FS-F) RVs, $Z_{\mathcal{F},1}$ and $Z_{\mathcal{F},2}$ can be mathematically given as:

$$Z_{\mathcal{F}} = Z_{\mathcal{F},1}/Z_{\mathcal{F},2} = (X_{n,1}Y_{In,1})/(X_{n,2}Y_{In,2}) = (X_{n,1}/Y_{n,1})/(X_{n,2}/Y_{n,2}) \tag{1}$$

where $X_{n,1}$ and $Y_{In,1}$ are Nakagami-m and inverse normalised Nakagami-m RVs given in (Yoo et al., 2017). Thus, the PDFs of $X_{n,1}$ and $Y_{n,1} = 1/Y_{In,1}$ are, respectively:

$$p_{X_{n,1}}(x_{n,1}) = \frac{2(\frac{m_{m,1}}{\Omega_1})^{m_{m,1}} x_{n,1}^{2m_{m,1}-1}}{\Gamma(m_{m,1})} e^{-m_{m,1}x_{n,1}^2} \tag{2}$$

$$p_{Y_{n,1}}(y_{n,1}) = \frac{2(m_{s,1}-1)^{m_{s,1}} y_{n,1}^{2m_{s,1}-1}}{\Gamma(m_{s,1})} e^{-(m_{s,1}-1)y_{n,1}^2} \tag{3}$$

where the multi-path and shadowing parameters are $m_{m,1}$ and $m_{s,1}$, respectively, whereas Ω_1 is the shaping parameter.

⋆ Corresponding author: danijel.djosic@pr.ac.rs

Similarly, the PDFs of the interference signals of Nakagami-m distribution $X_{n,2}$ (Hadzi-Velkov, 2007a) and normalised Nakagami-m $Y_{n,2}$, respectively can be given as:

$$p_{X_{n,2}}(x_{n,2}) = \frac{2(\frac{m_{m,2}N_m}{\Omega_2})^{m_{m,2}} x_{n,2}^{2m_{m,2}N_m-1}}{\Gamma(m_{m,2}N_m)} e^{-m_{m,2}x_{n,m}^2} \tag{4}$$

$$p_{Y_{n,2}}(y_{n,2}) = \frac{2((m_{s,2}-1)N_s)^{m_{s,2}} x_{n,2}^{(2m_{s,2}-1)N_s}}{\Gamma(m_{m,s}N_s)} e^{-(m_{s,2}-1)y_{n,2}^2} \tag{5}$$

where the CCI multi-path and shadowing parameters are $m_{m,2}$ and $m_{s,2}$, respectively, Ω_2 is the CCI shaping parameter, N_m and N_s characterize the number of interfers.

The PDF of the $Z_{\mathcal{F},1} = X_{n,1}/Y_{n,i}$, $i = 1, 2$ can be expressed as:

$$p_{Z_{\mathcal{F},i}}(z_{\mathcal{F},i}) = \int_0^\infty \left|\frac{dx_{n,i}}{dz_{\mathcal{F},i}}\right| p_{X_{n,i}}(z_{\mathcal{F},i}y_{n,i}) p_{Y_{n,i}}(y_{n,i}) dy_{n,i} \tag{6}$$

where $\left|\frac{dx_{n,i}}{dz_{\mathcal{F},i}}\right| = y_{n,i}$. Based on (1-4), and using (Gradshteyn & Ryzhik, 2014), the PDF of $Z_{\mathcal{F},1}(z_{\mathcal{F},1})$ can be written as:

$$p_{Z_{\mathcal{F},1}}(z_{\mathcal{F},1}) = \frac{2\left(m_{m,1}/\Omega_1\right)^{m_{m,1}} (m_{s,1}-1)^{m_{s,1}} \Omega_1^{m_{m,1}+m_{s,1}}}{B(m_{m,1}, m_{s,1})} \times \frac{z_{\mathcal{F},1}^{2m_{m,1}-1}}{\left(m_{m,1}z_{\mathcal{F},1}^2 + \Omega_1(m_{s,1}-1)\right)^{m_{m,1}+m_{s,1}}} \tag{7}$$

while $p_{Z_{\mathcal{F},2}}(z_{\mathcal{F},2})$ is:

$$p_{Z_{\mathcal{F},2}}(z_{\mathcal{F},2}) = \frac{2\left(m_{m,2}/\Omega_2\right)^{m_{m,2}N_m} (m_{s,2}-1)^{m_{s,2}N_s}}{B(m_{m,2}N_m, m_{s,2}N_s)} \times \frac{z_{\mathcal{F},2}^{2m_{m,2}N_m-1} \Omega_2^{m_{m,2}N_m+m_{s,2}N_s}}{\left(m_{m,2}z_{\mathcal{F},2}^2 + \Omega_2(m_{s,2}-1)\right)^{m_{m,2}N_m+m_{s,1}N_s}} \tag{8}$$

Similarly, the PDF of a ratio of FS-F RVs $Z_\mathcal{F} = Z_{\mathcal{F},1}/Z_{\mathcal{F},2}$ can be obtained from:

$$p_{Z_\mathcal{F}}(z_\mathcal{F}) = \int_0^\infty \left|\frac{dz_{\mathcal{F},1}}{dz_\mathcal{F}}\right| p_{Z_{\mathcal{F},1}}(z_\mathcal{F} z_{\mathcal{F},2}) p_{Z_{\mathcal{F},2}}(z_{\mathcal{F},2}) dz_{\mathcal{F},2} \tag{9}$$

where $\left|\frac{dz_{\mathcal{F},1}}{dz_\mathcal{F}}\right| = z_{\mathcal{F},2}$. Finally, PDF of $p_{Z_\mathcal{F}}(z_\mathcal{F})$ can be written as:

$$p_{Z_\mathcal{F}}(z_\mathcal{F}) = \frac{4{m_{m,1}}^{m_{m,1}}(m_{s,1}-1)^{m_{s,1}}}{B(m_{m,1}, m_{s,1})B(m_{m,2}N_m, m_{s,2}N_s)} \times {m_{m,2}}^{m_{m,2}N_m}(m_{s,2}-1)^{m_{s,2}N_s}\Omega_1^{m_{s,1}}\Omega_2^{m_{s,2}N_s} z_\mathcal{F}^{2m_m-1} \times \int_0^\infty \frac{z_{\mathcal{F},2}^{2m_{m,1}+2m_{m,2}N_m-1}}{(m_{m,1}(z_\mathcal{F} z_{\mathcal{F},2})^2 + (m_{s,1}-1)\Omega_1)^{m_{m,1}+m_{s,1}}} \times \frac{1}{(m_{m,2}z_{\mathcal{F},2}^2 + (m_{s,2}-1)\Omega_2)^{m_{m,2}N_m+m_{s,2}N_s}} dz_{\mathcal{F},2} \tag{10}$$

After using (Gradshteyn & Ryzhik, 2014), a closed-form PDF expression $p_{Z_\mathcal{F}}(z_\mathcal{F})$ of a ratio of two FS-F in terms of Gaussian hyper-geometric function ${}_2F_1(\cdot,\cdot;\cdot;\cdot)$ (Gradshteyn & Ryzhik, 2014) is derived and presented as (11) at the top of the next page.

The CDF of a ratio of FS-F RVs can be obtained from $F_{Z_\mathcal{F}}(z_\mathcal{F}) = \int_0^{z_\mathcal{F}} p_{Z_\mathcal{F}}(x)dx$. Thus, $F_{Z_\mathcal{F}}(z_\mathcal{F})$ can be given as:

$$F_{Z_\mathcal{F}}(z_\mathcal{F}) = \frac{4{m_{m,1}}^{m_{m,1}}(m_{s,1}-1)^{m_{s,1}}}{B(m_{m,1}, m_{s,1})B(m_{m,2}N_m, m_{s,2}N_s)} \times {m_{m,2}}^{m_{m,2}N_m}(m_{s,2}-1)^{m_{s,2}N_s}\Omega_1^{m_{s,1}}\Omega_2^{m_{s,2}N_s} \times \int_0^\infty dz_{\mathcal{F},2} \frac{z_{\mathcal{F},2}^{2m_{m,1}+2m_{m,2}N_m-1}}{(m_{m,2}z_{\mathcal{F},2}^2 + (m_{s,2}-1)\Omega_2)^{m_{m,2}N_m+m_{s,2}N_s}} \times \int_0^{z_\mathcal{F}} \frac{x^{2m_{m,1}-1}}{(m_{m,1}x^2 z_{\mathcal{F},2}^2 + (m_{s,1}-1)\Omega_1)^{m_{m,1}+m_{s,1}}} dx \tag{12}$$

The level crossing rate ($N_{z_\mathcal{F}}$) for the predetermined envelope threshold z_{th}, $N_{z_\mathcal{F}}(z_{th})$ can be given as:

$$N_{z_\mathcal{F}}(z_{th}) = \int_0^\infty \dot{z}_\mathcal{F} p_{z_\mathcal{F}\dot{z}_\mathcal{F}}(z_{th}, \dot{z}_\mathcal{F}) d\dot{z}_\mathcal{F} \tag{13}$$

where, $p_{z_\mathcal{F}\dot{z}_\mathcal{F}}(z_\mathcal{F}, \dot{z}_\mathcal{F})$ is the joint distribution of the signal-to-interference ratio (SIR) envelope, $z_\mathcal{F}$ and its first derivative $\dot{z}_\mathcal{F}$.

Since we can express the received SIR as $Z_\mathcal{F} = Z_{\mathcal{F},1}/Z_{\mathcal{F},2}$, where $Z_{\mathcal{F},1}$ and $Z_{\mathcal{F},2}$ can be further expressed as $Z_{\mathcal{F},1} = X_{n,1}Y_{In,1} = X_{n,1}/Y_{n,1}$ and $Z_{\mathcal{F},2} = X_{n,2}Y_{In,2} = X_{n,2}/Y_{n,2}$, respectively, the $p_{z_\mathcal{F}\dot{z}_\mathcal{F}}(z_{th}, \dot{z}_\mathcal{F})$ can be given as an integral-form expression of a joint PDF of independent and identically distributed (i.i.d) RVs, $Z_\mathcal{F}, \dot{Z_\mathcal{F}}, Y_{n,1}, X_{n,2}$ and $Y_{n,2}$, can be given as:

$$p_{z_\mathcal{F}\dot{z}_\mathcal{F}}(z_\mathcal{F}, \dot{z}_\mathcal{F}) = \int_0^\infty dy_{n,1} \int_0^\infty dx_{n,2} \times \int_0^\infty p_{z_\mathcal{F}\dot{z}_\mathcal{F}y_{n,1}x_{n,2}y_{n,2}}(z_\mathcal{F}\dot{z}_\mathcal{F}y_{n,1}x_{n,2}y_{n,2}) dy_{n,2} \tag{14}$$

where $p_{z_\mathcal{F}\dot{z}_\mathcal{F}y_{n,1}x_{n,2}y_{n,2}}(z_\mathcal{F}\dot{z}_\mathcal{F}y_{n,1}x_{n,2}y_{n,2})$ can be further simplified and expressed through independent conditional and individual PDFs as:

$$\begin{aligned} &p_{z_\mathcal{F}\dot{z}_\mathcal{F}y_{n,1}x_{n,2}y_{n,2}}(z_\mathcal{F}\dot{z}_\mathcal{F}y_{n,1}x_{n,2}y_{n,2}) \\ &\quad = p_{\dot{z}_\mathcal{F}|z_\mathcal{F}y_{n,1}x_{n,2}y_{n,2}}(\dot{z}_\mathcal{F}|z_\mathcal{F}y_{n,1}x_{n,2}y_{n,2}) \\ &\quad \times p_{z_\mathcal{F}y_{n,1}x_{n,2}y_{n,2}}(z_\mathcal{F}y_{n,1}x_{n,2}y_{n,2}) \\ &\quad = p_{\dot{z}_\mathcal{F}|z_\mathcal{F}y_{n,1}x_{n,2}y_{n,2}}(\dot{z}_\mathcal{F}|z_\mathcal{F}y_{n,1}x_{n,2}y_{n,2}) \\ &\quad \times p_{z_\mathcal{F}|y_{n,1}x_{n,2}y_{n,2}}(z_\mathcal{F}|y_{n,1}x_{n,2}y_{n,2}) \\ &\quad \times p_{y_{n,1}}(y_{n,1})\, p_{x_{n,2}}(x_{n,2})\, p_{y_{n,2}}(y_{n,2}) \end{aligned} \tag{15}$$

The conditional distribution $p_{z_\mathcal{F}|y_{n,1}x_{n,2}y_{n,2}}(z_\mathcal{F}|y_{n,1}x_{n,2}y_{n,2})$ is then transformed into:

$$p_{z_\mathcal{F}|y_{n,1}x_{n,2}y_{n,2}}(z_\mathcal{F}|y_{n,1}x_{n,2}y_{n,2}) = \left|\frac{dx_{n,1}}{dz_\mathcal{F}}\right| p_{x_{n,1}}\left(\frac{z_\mathcal{F}y_{n,1}x_{n,2}}{y_{n,2}}\right) \tag{16}$$

From (13-16), the $N_{z_\mathcal{F}}$ of SIR envelope threshold in FS-F propagation environments is expressed as:

$$\begin{aligned} N_{z_\mathcal{F}}(z_{th}) = &\int_0^\infty dy_{n,1} \int_0^\infty dx_{n,2} \int_0^\infty dy_{n,2} \\ &\times \left|\frac{dx_{n,1}}{dz_\mathcal{F}}\right| p_{x_{n,1}}\left(\frac{z_\mathcal{F}y_{n,1}x_{n,2}}{y_{n,2}}\right) \\ &\times p_{y_{n,1}}(y_{n,1})\, p_{x_{n,2}}(x_{n,2})\, p_{y_{n,2}}(y_{n,2}) \\ &\times \int_0^\infty \dot{z}_\mathcal{F} p_{\dot{z}_\mathcal{F}|z_\mathcal{F}y_{n,1}x_{n,2}y_{n,2}}(\dot{z}_\mathcal{F}|z_\mathcal{F}y_{n,1}x_{n,2}y_{n,2})\, d\dot{z}_\mathcal{F} \end{aligned} \tag{17}$$

$$p_{z_{\mathcal{F}}}(z_{\mathcal{F}})= \frac{2(m_{m,1}/\Omega_1)^{m_{m,1}}(m_{m,2}/\Omega_2)^{m_{m,2}}}{B(m_{m,1},m_{s,1})B(m_{m,2}N_m,m_{s,2}N_s)(m_{s,1}-1)^{m_{m,1}}(m_{s,2}-1)^{m_{m,2}N_m}} z_{\mathcal{F}}^{2m_{m,1}-1} B(m_{m,1}+m_{m,2}N_m, m_{s,1}+m_{s,2}N_s)$$
$$\times \left(\frac{m_{m,2}}{(m_{s,2}-1)\Omega_2}\right)^{-m_{m,1}-m_{m,2}N_m} \left({}_2F_1\left(m_{m,1}+m_{s,1}, m_{m,1}+m_{m,2}N_m; m_{m,1}+m_{s,1}+m_{m,2}N_m+m_{s,2}N_s; 1-\frac{m_{m,1}(m_{s,2}-1)\Omega_2 z_{\mathcal{F}}}{(m_{m,2})(m_{s,1}-1)\Omega_1}\right)\right) \quad (11)$$

where,

$$\int_0^\infty \dot{z}_{\mathcal{F}}\, p_{\dot{z}_{\mathcal{F}}|z_{\mathcal{F}}y_{n,1}x_{n,2}y_{n,2}}(\dot{z}_{\mathcal{F}}|z_{\mathcal{F}}y_{n,1}x_{n,2}y_{n,2})\, d\dot{z}_{\mathcal{F}} = \frac{\sigma_{\dot{z}_{\mathcal{F}}}}{\sqrt{2\pi}} \quad (18)$$

The $\sigma^2_{\dot{z}_{\mathcal{F}}}$ is the variance of $\dot{z}_{\mathcal{F}}$. Furthermore, $\dot{z}_{\mathcal{F}}$ can be written as:

$$\dot{z}_{\mathcal{F}} = \frac{y_{n,2}}{y_{n,1}x_{n,2}}\dot{x}_{n,1} - \frac{x_{n,1}y_{n,2}}{y^2_{n,1}x_{n,2}}\dot{y}_{n,1} - \frac{x_{n,1}y_{n,2}}{y_{n,1}x^2_{n,2}}\dot{x}_{n,2} + \frac{y_{n,1}}{y_{n,1}x_{n,2}}\dot{y}_{n,2} \quad (19)$$

where $\dot{x}_{n,1}$, $\dot{y}_{n,1}$, $\dot{x}_{n,2}$ and $\dot{y}_{n,2}$ are the first derivatives of $x_{n,1}$, $y_{n,1}$, $x_{n,2}$ and $y_{n,2}$, respectively. We assume that $\dot{z}_{\mathcal{F}}$ is a zero-mean Gaussian RV whose variance after some transformations can be expressed as:

$$\sigma^2_{\dot{z}_{\mathcal{F}}} = \frac{y^2_{n,2}}{y^2_{n,1}x^2_{n,2}}\sigma_{\dot{x}^2_{n,1}}\left(1 + \frac{z^2_{\mathcal{F}}x^2_{n,2}}{y^4_{n,2}}\frac{\sigma_{\dot{y}^2_{n,1}}}{\sigma_{\dot{x}^2_{n,1}}} + \frac{z^2_{\mathcal{F}}y^2_{n,1}}{y^2_{n,2}}\frac{\sigma_{\dot{x}^2_{n,2}}}{\sigma_{\dot{x}^2_{n,1}}} + \frac{z^2_{\mathcal{F}}y^2_{n,1}x^2_{n,2}}{y^4_{n,2}}\frac{\sigma_{\dot{y}^2_{n,2}}}{\sigma_{\dot{x}^2_{n,1}}}\right) \quad (20)$$

where $\sigma_{\dot{x}^2_{n,1}}$, $\sigma_{\dot{y}^2_{n,1}}$, $\sigma_{\dot{x}^2_{n,2}}$ and $\sigma_{\dot{y}^2_{n,2}}$ are the variances of $\dot{x}_{n,1}$, $\dot{y}_{n,1}$, $\dot{x}_{n,2}$ and $\dot{y}_{n,2}$, respectively. Finally, $N_{z_{\mathcal{F}}}(z_{th})$ of a SIR threshold envelope for $\sigma_{\dot{x}^2_{n,1}}=\pi^2 f_m^2(\Omega_1/m_{m,1})$ can be written as:

$$N_{z_{\mathcal{F}}}(z_{th})/f_m = \frac{16 m_{m,1}^{m_{m,1}-1/2}(m_{m,2}N_m)^{m_{m,2}}(m_{s,1}-1)^{m_{s,1}}}{\sqrt{2\pi}\Omega_m^{m_{m,1}-1/2}\Omega_s^{m_{s,1}}\Gamma(m_{m,1})\Gamma(m_{s,1})\Gamma(m_{m_2}N_m)} \times \frac{(m_{s,2}N_s-1)^{m_{s,2}}}{\Gamma(m_{s,2}N_s)} z_{th}^{2m_{m_1}-1} I_1 \quad (21)$$

where I_1 is provided as:

$$I_1 = \int_0^\infty dy_{n,1}\int_0^\infty dx_{n,2}\int_0^\infty dy_{n,2} \times \left(1 + \frac{z^2_{\mathcal{F}}x^2_{n,2}}{y^4_{n,2}}\frac{\sigma_{\dot{y}^2_{n,1}}}{\sigma_{\dot{x}^2_{n,1}}} + \frac{z^2_{\mathcal{F}}y^2_{n,1}}{y^2_{n,2}}\frac{\sigma_{\dot{x}^2_{n,2}}}{\sigma_{\dot{x}^2_{n,1}}} + \frac{z^2_{\mathcal{F}}y^2_{n,1}x^2_{n,2}}{y^4_{n,2}}\frac{\sigma_{\dot{y}^2_{n,2}}}{\sigma_{\dot{x}^2_{n,1}}}\right)^{\frac{1}{2}} \times x_{n,2}^{2m_{m_1}+2m_{s_1}-2} y_{n,1}^{2m_{m_2N_m}+2m_{m_1}-2} y_{n,2}^{2m_{s_2N_s}-2m_{m_1}} \times e^{-\frac{m_{m_1}}{\Omega_1}\frac{z^2_{th}y^2_{n,1}x^2_{n,2}}{y^2_{n,2}} - \frac{m_{m_2}}{\Omega_2}x^2_{n,2} - (m_{s_1}-1)y^2_{n,1} - (m_{s_2}-1)y^2_{n,2}} \quad (22)$$

Average fade duration (AFD), $A_{z_{\mathcal{F}}}(z_{th})$ is calculated as:

$$A_{Z_{\mathcal{F}}}(z_{th}) = \frac{F_{Z_{\mathcal{F}}}(z_{th})}{N_{Z_{\mathcal{F}}}(z_{th})} \quad (23)$$

where $F_{Z_{\mathcal{F}}}$ is provided in (12) and $N_{Z_{\mathcal{F}}}$ in (21).

NUMERICAL RESULTS

The first and second order statistics of the ratio of two FS-F RVs in terms of the PDF, LCR and AFD are presented on Figs 1-3. The $p_{z_{\mathcal{F}}}(z_{\mathcal{F}})$ for $\Omega_1 = \Omega_2 = 1$ and for various $m_{m,1}$, $m_{s,1}$, $m_{m,2}$, $m_{s,2}$ and $N = N_m = N_s$ is shown in Fig. 1. Normalised LCR, $N_{z_{\mathcal{F}}}(z_{th})/f_m$ is presented in Fig 2. for $\sigma_{\dot{x}^2_{n,1}}=\sigma_{\dot{y}^2_{n,1}}=\sigma_{\dot{x}^2_{n,2}}=\sigma_{\dot{y}^2_{n,2}}$ and $\Omega_1 = \Omega_2 = 1$, $N = N_m = N_s = 2$ and various values of m. It can be seen that by increasing values of m (shifting from more severe to less severe fading conditions), $N_{z_{\mathcal{F}}}(z_{th})$ decreases.

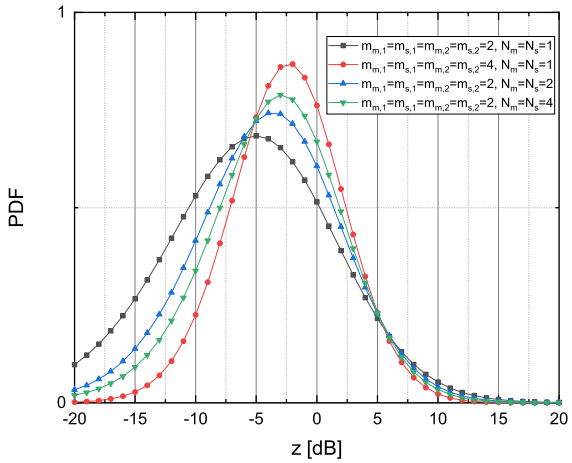

Figure 1. PDF for different m and N.

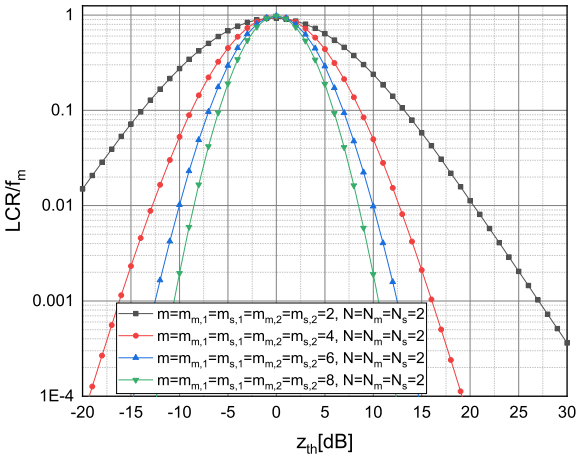

Figure 2. LCR for different m and $N = 2$.

Fig 3. shows $A_{Z_{\mathcal{F}}}(z_{th})f_m$ for $\Omega_1 = \Omega_2 = 1$ and for different m and $N = N_m = N_s$. It can be observed that by increasing values of m and N, the $A_{Z_{\mathcal{F}}}(z_{th})f_m$ decreases for lower values of z_{th} while increases for higher values of z_{th}. Moreover, the impact of N on $A_{Z_{\mathcal{F}}}(z_{th})f_m$ is more dominant for lower z_{th} while the impact of m on $A_{Z_{\mathcal{F}}}(z_{th})f_m$ is more dominant for higher z_{th}.

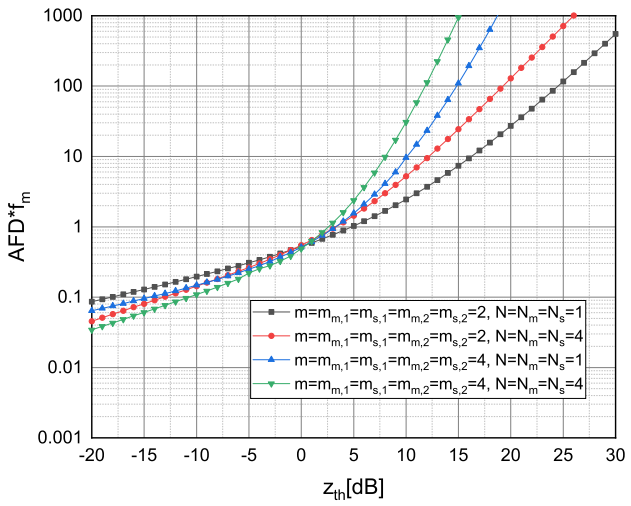

Figure 3. LCR for different m and N.

CONCLUSION

This paper investigates first and second order statistics of a ratio of two FS-F RVs in terms of $p_{Z_{\mathcal{F}}}(z_{\mathcal{F}})$, $F_{Z_{\mathcal{F}}}(z_{\mathcal{F}})$, $N_{Z_{\mathcal{F}}}(z_{th})$ and $A_{Z_{\mathcal{F}}}(z_{th})$. The system performance improvement can be achieved in less severe fading conditions (e.g., for higher values of m, LCR and AFD for lower values of z_{th} take lower values). In our future work we will consider SIR in relay and RIS systems over FS-F channels.

REFERENCES

Al-Hmood, H. & Al-Raweshidy, H. S. 2020, Selection combining scheme over non-identically distributed Fisher- Snedecor F fading channels, IEEE Wireless Communications Letters, 10(4), pp. 840-843. DOI: 10.1109/LWC.2020.3046519

Alshawaqfeh, M. K., Badarneh, O. S., & Almehmadi, F. S. 2022, Performance analysis of digital transmission in interferencelimited networks, Telecommunication Systems, 79(2), pp. 233-247.

Badarneh, O. S., Da Costa, D. B., Sofotasios, P. C., Muhaidat, S., & Cotton, S. L. 2018a, On the Sum of Fisher–Snedecor F Variates and Its Application to Maximal-Ratio Combining, IEEE Wireless Communications Letters, 7(6), pp. 966-969. DOI: 10.1109/LWC.2018.2836453

Badarneh, O. S., Muhaidat, S., Sofotasios, P. C., et al. 2018b, On the Secrecy Capacity of Fisher - Snedecor *F* Fading Channels, 14th International conference on wireless and mobile computing, networking and communications (WiMob), IEEE, pp. 1-7.

Badarneh, O. S., Sofotasios, P. C., Muhaidat, S., Cotton, S. L., & Da Costa, D. B. 2020, Product and ratio of product of Fisher-Snedecor variates and their applications to performance evaluations of wireless communication systems, IEEE Access, 8, pp. 215267-215286. DOI: 10.1109/ACCESS.2020.3039680

Cheng, W., Wang, X., Ma, T., & Wang, G. 2021, On the performance analysis of switched diversity combining receivers over Fisher–Snedecor composite fading channels, sensors, 21(9), pp. 3014. https://doi.org/10.3390/s21093014

Du, H., Zhang, J., Peppas, K. P., et al. 2019, On the Distribution of the Ratio of Products of Fisher-Snedecor F Random Variables and Its Applications, IEEE Transactions on Vehicular Technology, 69(2), pp. 1855-1866. DOI: 10.1109/TVT.2019.2961427

Gradshteyn, I. S. & Ryzhik, I. M. 2014, Table of integrals, series, and products (Academic press)

Hadzi-Velkov, Z. 2006, Level crossing rate and average fade duration of selection diversity with Rician-faded cochannel interferers, IEEE communications letters, 10(9), pp. 649-651. DOI: 10.1109/LCOMM.2006.1714533

Hadzi-Velkov, Z. 2007a, Level crossing rate and average fade duration of dual selection combining with cochannel interference and Nakagami fading, IEEE transactions on wireless communications, 6(11), pp. 3870-3876. DOI: 10.1109/TWC.2007.060206

Hadzi-Velkov, Z. 2007b, Second-Order Statistics of Selection Combining Systems with Cochannel Interference in Various Fading Channels, Proc. IEEE 18th International Symposium on Personal, Indoor and Mobile Radio Communications 2007 (PIMRC 2007), Athens, Greece.

Kong, L. & Kaddoum, G. 2018, On physical layer security over the Fisher-snedecor {*F*} wiretap fading channels, IEEE Access, 6, 39466–39472

Makarfi, A. U., Rabie, K. M., Kaiwartya, O., et al. 2020, Physical layer security in vehicular networks with reconfigurable intelligent surfaces. In 2020 IEEE 91st Vehicular Technology Conference (VTC2020-Spring), pp. 1–6. IEEE (2020), https://doi.org/10.1109/VTC2020-Spring48590.2020.9128438

Milosevic, N., Stefanovic, C., Nikolic, Z., Bandjur, M., & Stefanovic, M. 2018a, First-and second-order statistics of interference-limited mobile-to-mobile Weibull fading channel, Journal of Circuits, Systems and Computers, 27(11), 1850168. https://doi.org/10.1142/S0218126618501682

Milosevic, N., Stefanovic, M., Nikolic, Z., Spalevic, P., & Stefanovic, C. 2018b, Performance analysis of interference-limited mobile-to-mobile – fading channel, Wireless Personal Communications, 101, pp. 1685-1701.

Đošić, D., Milić, D., Kontrec, N., et al. 2022, Analytical performance analysis of the M2M wireless link with an antenna selection system over interference limited dissimilar composite fading environments, International Journal of Applied Mathematics and Computer Science, 32(4), pp. 569-582. https://doi.org/10.34768/amcs-2022-0040

Stefanovic, C., Djosic, D., Stefanovic, D., Milosevic, H., & Panic, S. R. 2022a, On the Second Order Statistics of Cooperative UAV Communications underlying Interference Limited Composite Fading Conditions, 18th International Conference on Wireless and Mobile Computing, Networking and Communications (WiMob), IEEE, pp. 400-405.

Stefanovic, C., Morales-Céspedes, M., & Armada, A. G. 2021a, Performance analysis of RIS-assisted FSO communications over Fisher–Snedecor F turbulence channels, Applied Sciences, 11(21), 10149. https://doi.org/10.3390/app112110149

Stefanovic, C., Morales-Céspedes, M., Róka, R., & Armada, A. G. 2021b, Performance analysis of N-Fisher- Snedecor F fading and its application to N-hop FSO communications. In Proceedings of the 17th IEEE International Symposium on Wireless Communication Systems (ISWCS), Berlin, Germany.

Stefanović, Č., Panić, S., Djosić, D., Milić, D., & Stefanović, M. 2021, On the second order statistics of N-hop FSO communications over N-gamma-gamma turbulence induced fading channels, Physical Communication, 45, 101289, https://doi.org/10.1016/j.phycom.2021.101289

Stefanovic, C., Veljkovic, S., Stefanovic, M., Panic, S., & Jovkovic, S. 2018, Second Order Statistics of SIR based Macro Diversity System for V2I Communications overComposite Fading Channels, First International Conference on Secure Cyber Computing and Communication (ICSCCC), IEEE, pp. 569-573.

Stefanovic, C. M., Armada, A. G., & Costa-Pérez, X. 2022b, Second Order Statistics of-Fisher-Snedecor Distribution and Their Application to Burst Error Rate Analysis of Multi-Hop Communications, IEEE Open Journal of the Communications Society, 3, pp. 2407-2424. DOI: 10.1109/OJCOMS.2022.3224835

Stefanović, M., Panić, S. R., Stefanović, D., Nikolić, B., & Cvetković, A. 2012, Second order statistics of selection combining receiver over - fading channels subject to co-channel interferences, Radio Science, 47(06), pp. 1-8.

Suljović, S., Milić, D., Panić, S., Stefanović, Č., & Stefanović, M. 2020, Level crossing rate of macro diversity reception in composite Nakagami-m and Gamma fading environment with interference, Digital Signal Processing, 102, 102758.

Yao, Z., Cheng, W., Zhang, W., & Zhang, H. 2021, Resource allocation for 5G-UAV-based emergency wireless communications, IEEE Journal on Selected Areas in Communications, 39(11), pp. 3395-3410. DOI:10.1109/jsac.2021.3088684

Yoo, S. K., Cotton, S. L., Sofotasios, P. C., et al. 2017, The Fisher–Snedecor F Distribution: A Simple and Accurate Composite Fading Model, IEEE Communications Letters, 21(7), pp. 1661-1664. DOI: 10.1109/LCOMM.2017.2687438

Yoo, S. K., Cotton, S. L., Sofotasios, P. C., Muhaidat, S., & Karagiannidis, G. K. 2019, Level Crossing Rate and Average Fade Duration in F Composite Fading Channels, IEEE Wireless Communications Letters, 9(3), pp.281-284. DOI: 10.1109/LWC.2019.2952343

Zhang, P., Du, H., Cao, Y., & Zhang, J. 2019, Wireless Powered UAV Relay Communications over the Fisher- Snedecoer f Fading Channels, IEEE 90 th Vehicular Technology Conference (VTC2019-Fall), IEEE, pp. 1-5.

Zhang, P., Zhang, J., Peppas, K. P., Ng, D. W. K., & Ai, B. 2020, Dual-hop relaying communications over Fisher- Snedecor F-fading channels, IEEE Transactions on Communications, 68(5), pp. 2695-2710.

CIP - Каталогизација у публикацији
Народна библиотека Србије, Београд

5

BULLETIN of Natural Sciences Research / editor in chief Stefan R. Panić. - [Štampano izd.]. - Vol. 10, no. 2 (2020)- . - Kosovska Mitrovica : Faculty of Sciences and Mathematics, University of Priština, 2020- (Kruševac : Sigraf). - 29 cm

Polugodišnje. - Je nastavak: The University thought. Publication in natural sciences = ISSN 1450-7226. – Drugo izdanje na drugom medijumu: Bulletin of Natural Sciences Research (Online) = ISSN 2738-1013
ISSN 2738-0971 = Bulletin of Natural Sciences Research (Štampano izd.)
COBISS.SR-ID 28586505

Available Online

This journal is available online. Please visit http://www.bulletinnsr.com to search and download published articles.